

Review

Theories on Frustrated Electrons in Two-Dimensional Organic Solids

Chisa Hotta

Department of Physics, Kyoto Sangyo University, Kita-ku Kamigamo Motoyama, Kyoto 603-8555, Japan; E-Mail: chisa@cc.kyoto-su.ac.jp

Received: 28 April 2012; in revised form: 9 July 2012 / Accepted: 26 July 2012 /

Published: 20 August 2012

Abstract: Two-dimensional quarter-filled organic solids are a promising class of materials to realize the strongly correlated insulating states called dimer Mott insulator and charge order. In their conducting layer, the molecules form anisotropic triangular lattices, harboring geometrical frustration effect, which could give rise to many interesting states of matter in the two insulators and in the metals adjacent to them. This review is concerned with the theoretical studies on such issue over the past ten years, and provides the systematic understanding on exotic metals, dielectrics, and spin liquids, which are the consequences of the competing correlation and fluctuation under frustration.

Keywords: frustration; strongly correlated electron; quantum spin system; dielectrics; triangular lattice

1. Introduction

The study on “*frustrated*” systems dates back to 1950, when Wannier found an exact solution of the triangular lattice Ising antiferromagnet [1]. Long afterward in 1977, Toulouse [2] introduced the term “*frustration*” in the field of condensed matter to describe a spin glass based on a plaquette motif with energetically unsatisfied bonds. The frustration in magnets has a very simple geometric origin, but nonetheless, it continued to develop new spin texture or non-magnetic objects/states, such as spirals, spin ices, spin liquids, valence bond solids, monopoles, quadrupoles (nematic orders), *etc.*, throughout its history [3]. Thus, the consequences of frustration have been studied in the realm of the localized spin systems, and far less attention was paid to those of the electronic systems until very recently. The latter relatively unstudied issue is what the present review focuses on.

The electronic systems have the charge and the orbital degrees of freedom besides the spins. If each electron is localized on a single atomic orbital, the system is reduced to the above mentioned magnets with short range interactions. However, as the charges fluctuate between different orbitals, the spins couple to the orbital degrees of freedom. Further, when electrons start to delocalize, the charge degrees of freedom play a major role. Thus, either the spin exchange interactions, coupled orbital-spin exchanges, and the Coulomb interactions, or their combinations come into play, depending on their energy scales. Frustration could work on all of them, which is the key distinction from the simple magnets. In the normal metallic state well described in reciprocal-space, the frustration often based on the real space geometry of interactions is not of direct importance. For this reason, the insulating states driven by the strong correlation and the metallic states in their very vicinity are our main focus, wherein the frustration effect is amenable to laboratory studies.

Two-dimensional organic solids could offer great possibility on this matter because of the following potentials they hold; they reveal a class of insulators called the charge order and the dimer Mott, which are the consequences of strong electronic interactions and of their particular carrier number called “quarter-filling”. Besides, the molecules in the conducting layers provide a variety of lattice geometry, which are mostly based on a triangular motif, reminiscent of the geometrical frustration. Thus, the two insulating states, when exposed under the frustration effect, yield many interesting and often exotic phenomena. Many theories and experiments during this decade could indeed be understood in this context.

In the present article, the term “strong coupling” refers to the electronic interactions being far stronger than the kinetic energy scale, and the “weak coupling” to the opposite case. The plan of this review is as follows. In Section 2 we give an overview of rich physics of organic solids under strong and frustrated electronic interactions, together with some preliminary informations before launching into the review. Section 3 explains three different classes of frustrated states realized in the strong coupling regime, *frustrated metals*, *dielectric insulators*, and *a spin liquid Mott insulator*. In Section 4, we explain several theories based on weak-coupling analyses, which are motivated by the experimental studies on organic crystals. We pick up some of the recent experimental findings on molecule-based materials related to frustration in Section 5, and then finalize the review at Section 6.

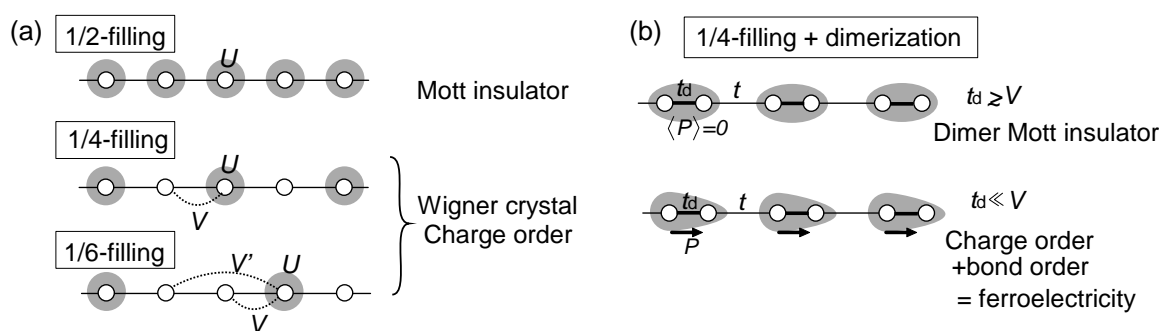
2. Preliminaries

2.1. Physics Relevant in Two Dimensional Organic Crystals

In lattice models with long range interactions, the electrons may localize to maximally avoid each other, when the commensurability of the carrier number to the lattice is satisfied. A classical sketch in Figure 1(a) helps to know that the electrons at a filling of $N_e/N = 1/m$ (m is an integer, N_e is the electron number, and N is the number of lattice sites) need the Coulomb interactions ranging from the on-site to over more than $(m - 1)$ -lattice spacing, in order to form “a Wigner crystal on a lattice” in analogy to the electron gas. The one at half-filling ($m = 1$) is called “Mott insulator”, and others are referred to as “charge ordering”. Noteworthy here is the crucial role of the commensurability pinning (effect of periodic potentials formed by the lattice), to suppress the quantum fluctuation against the

interaction. In fact, Noda and Imada showed in two-dimension that the critical interaction strength for Wigner crystallization is significantly lowered from those of electron gas to the realistic values in lattice models at some special fillings, $m = 1, 2$ and 3, but no longer at larger m (lower electron density) [4]. The critical value at $m = 2$ is as small as to be reproduced even by the mean-field solution, and thus, the quarter-filled ($m = 2$) organic systems are allowed to display this interaction-driven insulating state particularly easily [5].

Figure 1. Schematic illustration of the insulating states on a lattice at $1/(2m)$ -filling (*i.e.*, the electron density, $N_e/N = 1/m$), driven by the strong Coulomb interactions and by the strong commensurability of the lattice. **(a)** Mott insulator ($m = 1$) and charge orderings ($m = 2, 3$); **(b)** Dimer Mott insulator and coexistent state of charge order and dimerization at $m = 2$ (quarter-filling) are shown.

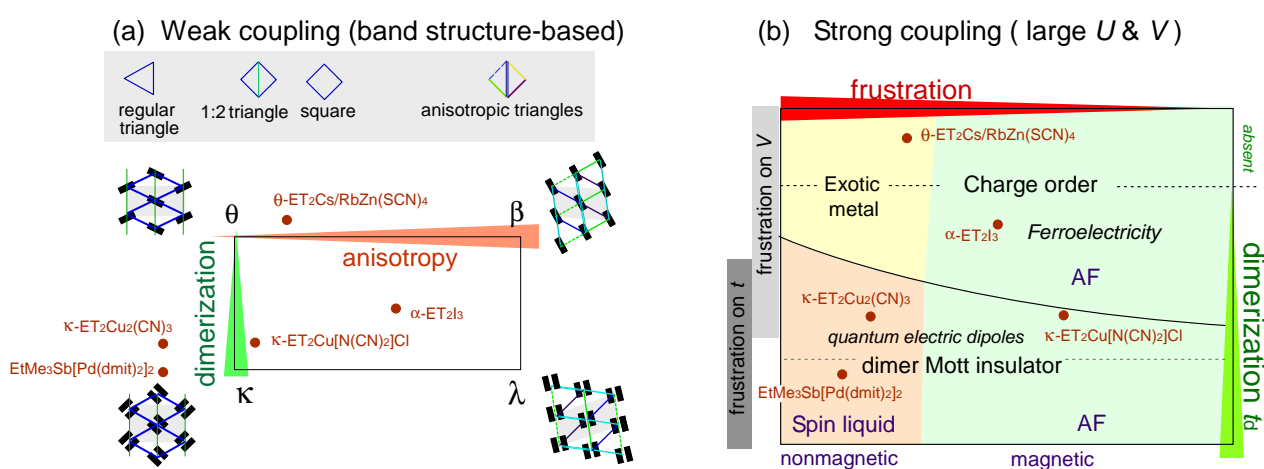


The “quarter-filling” of electrons is typically realized in a family of organic materials called charge transfer salts consisting of two kinds of molecules, A and B , in a 2:1 ratio. In such “ A_2B compounds”, the two-dimensional conducting A -layers have 1.5 electrons per one A -molecule on an average, *i.e.*, three-quarter-filling of electrons, or quarter-filling in terms of holes. At this filling, another special crystallization could occur besides the above mentioned charge order (see Figure 1(b)); when the molecules are strongly dimerized, the $m = 1$ electron crystal *in unit of dimerized molecules* emerges as a “dimer Mott insulator” [6]. There are also cases where the charge ordering and the dimerization (bond order) coexist, which give rise to ferroelectricity. The details of the variety of physics of quarter-filled organics are already reviewed in [7], and here we focus on more specific cases where the strong correlation due to frustration effect works on the two insulating states in a nontrivial manner.

Let us present an overall picture of what we could expect in these material systems. The band structures in the non-interacting limit provides the starting point to understand the features of each actual organic material. They are complicated due to a variety of transfer integrals (t), which reflect their molecular arrangements called polytypes. Hotta has already extracted the main factors governing their band structures, and classified the polytypes against these factors, *dimerization* and *anisotropy*, as shown in Figure 2(a) [8]; the molecules in θ - and β -types form anisotropic triangular lattices, just as the dimerized pair of molecules do in κ - and λ -types. The bonds (transfer integrals) of these triangles are not uniform: θ - and κ -types are somewhat special since the bonds take only two different values. The other polytypes are less symmetric and form a *highly anisotropic* triangular lattice. A strong dimerization is discriminated from other “anisotropy” in the sense that at quarter-filling, a dimer Mott insulator is

available. This classification has turned out to be effective when the interaction is weak, since it takes full account of the features of their one-particle states.

Figure 2. (a) The classification of quarter-filled electronic system in the weak-coupling regime. The θ and β -type with no (or weak) dimerization forms a triangular lattice in unit of molecule, whereas those with strong dimerization, κ - and λ -type do so in unit of dimer; (b) The overall sketch of the electronic states in the strong-coupling regime under frustration classified by the degree of dimerization, t_d . The axis of “anisotropy” of the crystals in (a) can be approximately interpreted as a degree of geometrical frustration here, when one accounts for t and V along the nearest neighbor bonds along the crystal lattices, at under the weak and strong dimerization, respectively.



Now, if we consider a strong inter-molecular Coulomb interactions, V , the “anisotropy” of these polytypes could govern the degree of geometrical frustration of V 's. For a moment, we focus on a strong coupling regime and overview three possible frustration-induced states shown schematically in Figure 2(b). The dimerization strength, represented by t_d , rules what degrees of freedom participate in the frustration effect. When the dimerization is absent, the charge degrees of freedom under competing V and t matters; the frustration effectively weakens the value of V , destroys the charge ordered insulator and will produce *an exotic metallic state*, in which the electrons may sometimes be not as mobile as in a usual metal.

As the dimerization (t_d) develops, the electron becomes confined within the dimer (dimer Mott insulator), but is still delocalized within the dimer, giving rise to *dielectric* degrees of freedom we call “quantum electric dipole”. The fluctuation and correlation of such electric moment are governed by t_d and V , respectively. They start to compete as the frustration weakens V , resulting in an unusual dielectric properties, which may sometimes yield a nontrivial magnetism through the exchange couplings of spins stucked to those dielectric moments.

Further stronger dimerization will effectively kill the dielectric moments, and the spin degrees of freedom start to play a major role. This time, by weakening the interaction strength, and in approaching the metal-insulator boundary (not shown), the virtual spacial fluctuation (by t) of electrons develops and

inter-site Coulomb interactions respectively, and t_{ij} is the transfer integral between sites i and j . We treat V_{ij} as those between nearest neighbor molecules (sites) unless otherwise noted.

In molecular solids, the roles played by atomic orbitals in inorganics are replaced with those by molecular orbitals, whereby the transfer integrals are the overlaps of molecular orbitals often provided by the extended Hückel method [9]. These empirical values were successful in reproducing the band structures of the first principle calculations in the first place [10], but often turned out to differ from the experimentally extracted values [11]. Lately, a density functional theory (DFT) revealed a bulk low energy band structure of κ -ET salts including the interaction effects to some extent [12,13]. Their evaluations on t 's somewhat deviate from the ones obtained by the extended Hückel method [14].

The estimate of the Coulomb interactions is more challenging. Empirical quantum chemistry calculations are performed [15,16]. A DFT on a single ET-molecule in a vacuum also provides a bare interactions as, $U^{\text{bare}} \sim 4 - 4.5$ eV [17], rather smaller than the ones from the quantum chemistry [16]. Still, these values are as large as $U^{\text{bare}}/t \sim 40$, and their reliability is controversial. Indeed, it is discussed in [16] that the values of about $U \sim 0.8-1.0$ eV and $V/U \sim 0.25$ are expected from various experiments. One direction to elucidate the realistic values is to compare the model calculations with the experimental data. Mila succeeded in determining the parameters of the quasi-one-dimensional Bechgaard salts (TMTSF/TMTTF molecules) from the optical data as, $U/t \sim 5-7$ and $V/t \sim 2-3$ [18]. Another development is the ab-initio DFT down-folding technique, which takes in the effect of screening from the energy bands off the target bands (targets are those near the Fermi level included in the Hubbard models) to the interaction values [13]. The evaluation onto κ -ET systems ranges in $U_{\text{eff}}/t_{\text{eff}} \sim 10-15$, $V_{\text{eff}}/U_{\text{eff}} \sim 0.2-0.5$, with $U_{\text{eff}} \sim 0.8$ eV, which are reduced by a factor of five from U^{bare} , but are still definitely in a strong coupling regime. Note that the downfolding estimation of $U_{\text{eff}}/t_{\text{eff}}$ is somewhat larger than expected (see the discussions in [13]), since when applied to the corresponding half-filled Hubbard model (see Figure 16 in Section 3.4), it will take the system deep inside the Mott insulating phase, which is contradictory with the experimental results on these κ -ET systems.

Going back to the models, one way to simplify the problem is to neglect the spin degrees of freedom, by reducing the extended Hubbard model to a t - V model of spinless fermions,

$$\mathcal{H}_{tV} = \sum_{\langle i,j \rangle} \left(-t_{ij}c_i^\dagger c_j + \text{H.c.} + V_{ij}n_i n_j \right) \quad (2)$$

The physical situation of three electrons (one hole) per two sites implies a half-filled band of spinless fermions, *i.e.*, one fermion per site with no double occupancy. This approximately corresponds to taking $U = \infty$ in the extended Hubbard model [19]. Note, however, that the weak coupling (small- U) region of the extended Hubbard model is not properly recovered because the band filling is twice as that of the spinful case.

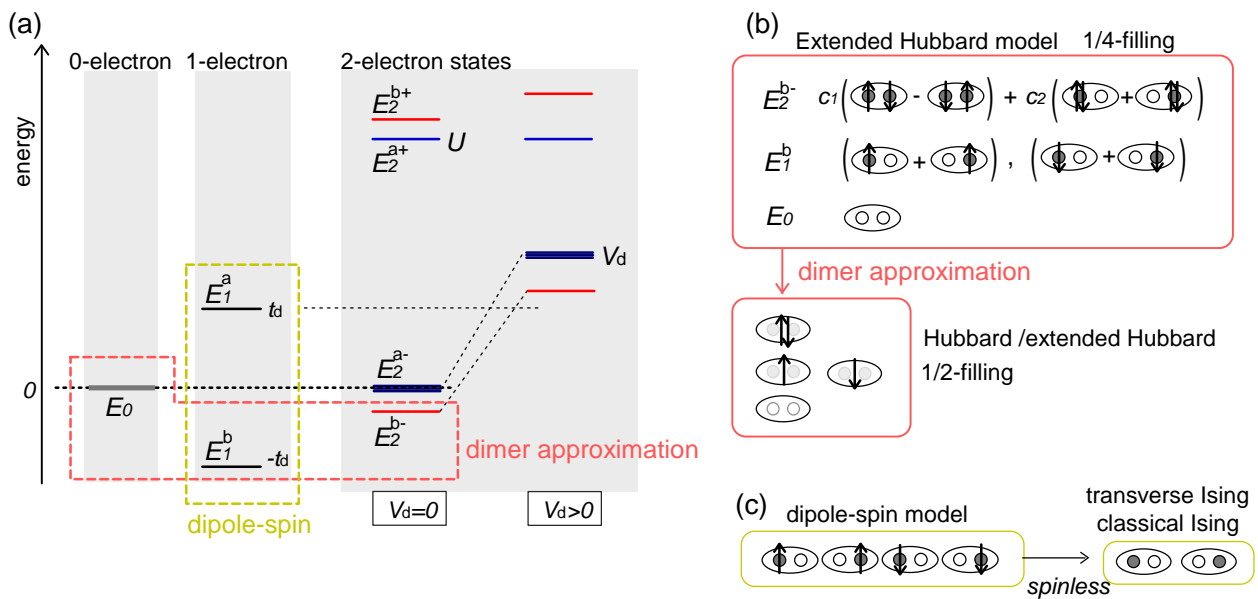
The strong coupling limit of the t - V model, $V_{ij}/t_{ij} = \infty$, is the Ising model in terms of classical particles,

$$\mathcal{H}_{\text{ising}} = \sum_{i,j} V_{ij} \left(n_i - \frac{1}{2} \right) \left(n_j - \frac{1}{2} \right) = \sum_{i,j} V_{ij} n_i n_j - \mu \sum_i n_i + \text{const} \quad (3)$$

where the particle number n_i is allowed to take only the discrete values, 0 or 1. The second term of the R.H.S. is added as a chemical potential (μ) term to the $t_{ij} = 0$ -limit of the t - V model in order to keep

the particle-hole symmetry, which amount to $-\mu \sum_i n_i + \text{const} = -N(2V + V')/4$, with $\mu = 2V + V'$ in the anisotropic triangular lattice model.

Figure 4. (a) Energy levels of zero ($E_0 = 0$), one ($E_1^{a/b} = \pm t_d$), and two electron states $E_2^{a\pm/b\pm}$ in the isolated dimer with $U \gg V_d$ and t_d . The approximation to the half-filled Hubbard model (dimer approximation) corresponds to confining the basis of a dimer to those belonging to E_0, E_1^b, E_2^{b-} . The dipole-spin model is verified in cases where all the two electron levels, $E_2^{a\pm/b\pm}$, become higher than $E_1^{a/b}$. Schematic illustration of the basis sets of the two approximations are shown in (b) and (c).



To capture another important aspect of the extended Hubbard model, we introduce an intrinsic (non-spontaneous) dimerization, represented by the large intra-dimer transfer integral, t_d . It is natural to look at the system in such a way that the dimers serve as a unit of a lattice instead of the sites.

On a dimer unit, there are sixteen basis states, as a doubling of the four basis states of a single site, $(\circ), (\uparrow), (\downarrow), (\uparrow\downarrow)$, where \circ and \uparrow represent the absence of electron and the up spin electron, respectively. Among them, the one with more than three electrons have high energy at large U and thus can be neglected. Figure 4(a) shows the energy levels, $E_n^{a/b}$, of n -electron energy ($n = 0, 1, 2$), where superscript a/b denotes the anti-bonding/bonding state. Let us further simplify the model within the remaining basis states by eliminating the relatively higher energy degrees of freedom within them. In the case of $V_d = 0$ (and $V_{ij} = 0$), a half-filled single band Hubbard model

$$\mathcal{H}_{\text{eff}} = \sum_{\langle i,j \rangle} \left(\sum_{\sigma} (-t_{\text{eff}} c_{i\sigma}^{\dagger} \tilde{c}_{j\sigma} + \text{H.c.}) \right) + \sum_i U_{\text{eff}} \tilde{n}_{i\uparrow} \tilde{n}_{i\downarrow} \quad (4)$$

is derived by taking the four lowest eigen-energy-states of zero- (E_0^b), one- (two E_1^b 's) and two-electrons (lower E_2^b), shown in Figure 4(a,b), and regarding them as a new basis, which process is called the “dimer approximation”. The operator $\tilde{c}_{i\sigma}^{\dagger}/\tilde{c}_{i\sigma}$ creates/annihilates the electron on these new levels. The on-dimer Coulomb interaction is obtained within this new basis as a “one particle charge gap” of the isolated dimer, $U_{\text{eff}} = E_0 + E_2^{b-} - 2E_1^b = 2t_d + \frac{U}{2} \pm \sqrt{\frac{U^2}{4} + 4t_d^2}$. (In the hole picture, $U_{\text{eff}} = \min(E_4) +$

$\min(E_2) - 2\min(E_3)$ gives the same result). So far, the upper bound of the above formula, $U_{\text{eff}} \sim 2t_d$, at $U = \infty$ (i.e., at $E_2^{b-} = 0$, which is an upper bound of this level) had often been applied as the effective interaction strength in material systems. However, once we set $V_d > 0$, the above discussion may easily break down. There are two problems. Firstly, the on-dimer Coulomb interactions are modified to

$$U_{\text{eff}} = 2t_d + \frac{U + V_d}{2} - \sqrt{\frac{(U - V_d)^2}{4} + 4t_d^2} \quad (5)$$

and for realistic values of U and V_d , this naturally exceeds the empirical estimation, $2t_d$, adopted to materials. The second problem is more serious. The energy level, E_2^{b-} , included in the dimer approximation shifts upward by V_d to near E_1^a . Therefore, discarding the anti-bonding one-electron state of E_1^a in the dimer approximation itself, even using Equation (5), may no longer be valid.

Straightforward way to avoid these problems is to further make $V_d \rightarrow \infty$, i.e., $U_{\text{eff}} \rightarrow \infty$, pushing all the two electron levels high up, and exclude the doubly occupied states on a dimer. Then, at a filling of one electron per dimer, the metallic state which requires double occupancy of dimer is no longer taken account of. The sixteen basis states of the extended Hubbard model is reduced to four again, but by a different choice from the above dimer approximation as shown in Figure 4(c); a single electron can be in either site of the dimer, which is the orbital degrees of freedom described by the dipole operator on m -th dimer, $P_m^z = \pm 1/2$. The quantization z -axis of dipoles is fixed to the dimer-bond direction in real space. Including the spin degrees of freedom, S^z , the four basis states in Figure 4(c) are described as, $(P^z, S^z) = (\pm \frac{1}{2}, \pm \frac{1}{2})$. The first order perturbation in the extended Hubbard model from the strong coupling limit, $U = V_d = \infty$, by $t_d > 0$ yields [20],

$$\mathcal{H}_{\text{tri}} = \sum_{\langle m,n \rangle} \tilde{V}_{mn} P_m^z P_n^z + \sum_m t_d (P_m^+ + P_m^-) \quad (6)$$

which is nothing but a transverse Ising model. Here, \tilde{V}_{mn} is the linear combination of V_{ij} 's connecting the sites i and j each belonging to two adjacent dimers, m and n , respectively. By the hopping (t_d) of electron, P_m^z flips quantum mechanically between $+1/2$ and $-1/2$, thus this object is regarded as a quantum electric dipole.

In Equation (6), all the spin configurations were degenerate, which is lifted by a higher order perturbation from the extended Hubbard model. The second order perturbation in terms of $t_{ij} > 0$ ($\neq t_d$) gives,

$$\mathcal{H}_{\text{KK}} = \sum_{\langle m,n \rangle} \left(W_0 S_m \cdot S_n - W_z (P_m^z P_n^z) (S_m \cdot S_n) + W_{xy} (P_m^+ + P_m^-) (S_m \cdot S_n) \right). \quad (7)$$

Besides the first Heisenberg term, the direct coupling of dipolar and spin degrees of freedom appears. Particularly, the second term reminds of a Kugel–Khomskii Hamiltonian studied in manganites [21]. Such direct couplings are mediated by the hopping of electrons to the nearest neighbor dimers, which we see later in Section 3.3 (Figure 15(c)). We call the combination of Equations (6,7) the dipole-spin model [20].

All the above models described in Figure 3 aim to capture the electronic correlation from the moderate to strong-coupling regime, whilst another important energy scale, an electron-lattice coupling, comes into play in the weak coupling regime, $t_{ij} \gtrsim U, V_{ij}$. Typically, the Holstein- and Peierls-type

(equivalently, Su–Schrieffer–Heeger-type) of electron-lattice interactions shall be relevant in organic crystals due to the anionic potential, or to the electron-molecular-vibration-coupling, which have the form,

$$\begin{aligned}\mathcal{H}_P &= -g_P \sum_{\langle ij \rangle} (u_i - u_j) t_{ij} (c_{i\sigma}^\dagger c_{j\sigma} + \text{H.c.}) + \sum_i \frac{K_P}{2} \sum_i u_i^2 \\ \mathcal{H}_H &= -g_H \sum_i v_i n_i + \frac{K_H}{2} \sum_i v_i^2\end{aligned}\quad (8)$$

where g 's and K 's are the coupling and elastic constants, respectively. The lattice displacements from their equilibrium position are described by the classical variables, u_i , v_i . Besides these terms, the anharmonic terms (those proportional to v_i^4 , u_i^4) are sometimes required to guarantee the existence of proper solutions with finite lattice distortions. The role of the electron-lattice couplings is reviewed in Section 4.

2.3. Frustration

We present here some introductory key issues in frustrated systems. The system is “frustrated” whenever it cannot minimize its total energy without sacrificing some of the local interaction energies. To be phenomenological, the “frustrated system” shall be characterized by the dense low energy structure of its many body states. The simplest way to capture it is to put the classical particles on the vertices of a unit of triangle or a square and count their energies according to Equation (3). If the two particles locate in both edges of a solid/broken bond, the repulsive/attractive interaction $V_{ij} = V$ between them raises/lowers the energy. A triangle and a square with odd number of attractive bonds (the one discussed by Toulouse [2]) shown in Figure 5(a) have a number of degenerate configurations. This degeneracy is a source of classical frustration. Indeed, when many triangles are condensed to form an edge-sharing triangular lattice, or a corner-shared Kagome lattice, a massive level of configurational disorder appears, resulting in an extensive ground state entropy [1,22].

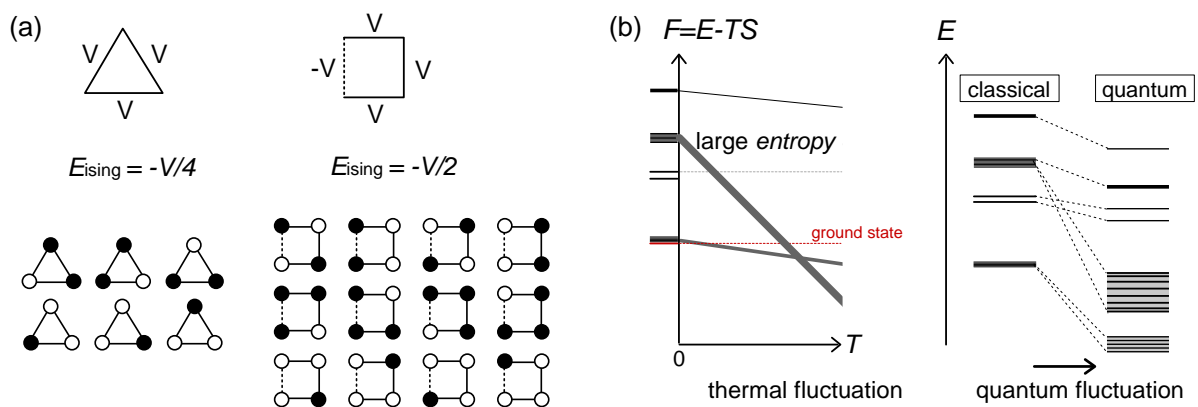
Note here that restricting the discussion to the nearest neighbor (local) interactions is not intrinsic. The classical degeneracy occurs on a geometrically unfrustrated square lattice when the longer range interactions are added. In fact, it is known that the localized spin systems with long range exchange interactions are intrinsically frustrated, irrespective of the lattice dimensionality or geometry of the lattice [23]. Similar picture is thus expected for the electronic system with unscreened long range Coulomb interactions, as we discuss shortly (Section 3.2).

One of the highlights in frustrated systems is an “order by disorder mechanism” [24]; an infinitesimally small perturbation favors a set of states among the degenerate manifolds, removing fully/partially the degeneracy of the low energy states. Figure 5(b) gives some sketches of the reconstruction of energy levels due to thermal and quantum fluctuations, represented by the temperature, T , and the electron hopping, t_{ij} , respectively. These effects are the origins of the exotic metallic states in Section 3.1.

In the frustrated systems, a severe competition among such dense low energy states often make it extremely difficult to determine the stable lowest energy states. Then, the above classical Ising particle system provides “the controlled limit” (see the beginning of Section 2.2), in which the geometrically

frustrated interactions are primarily taken account of, and thus the origin and the energy scales of the competing states are clarified. In contrast, from a weak coupling point of view, this problem is being rather blurred; if one extends the mean-field solutions—treating interactions in the lowest order as a one-body term—toward a regime of stronger and frustrated interaction, one sometimes encounters a case where the ground state cannot be safely determined from among several different solutions with almost degenerate energies. Even if one tries to choose one of them, it is not often stable against the inclusion of the correlation effect, namely a number of low energy excited states could easily take over it. In the next section, the readers will find several examples; exotic frustrated metals, spin liquid state, *etc.*, which cannot be captured by the mean-field solutions.

Figure 5. (a) Frustrated units of square and triangle with an Ising interaction $\pm V$ (solid/broken line) along their edges, and their lowest energy states. Filled/open circle is the presence/absence of classical particle. Lower panels represent the degenerate configurations; (b) Sketch of two types of reconstruction of energy levels due to thermal and quantum fluctuation, called “order by disorder” mechanism.



3. Strong Coupling Regime

Besides the basic extended Hubbard model at 3/4-filling, we apply the strong coupling effective models to focus on the role of frustration. In the first part, the topics on frustrated metals are discussed by the spinless Ising and t - V models at half-filling. The quantum electronic dielectrics due to orbital (intra-dimer) degrees of freedom is described by the dipole-spin model in the second part. The final topic on spin liquid Mott insulator aims to understand the connections of the half-filled Hubbard model to the localized spin systems.

3.1. Frustrated Metal: Ground States

The charges are frustrated when their inter-site Coulomb interactions compete with each other. A good starting point to understand such effect is the Ising model of classical and spinless particles in Equation (3) on an anisotropic triangular lattice, with two-different types of nearest-neighbor interactions, $V_{ij} = V$ and V' , along two diagonal directions and one vertical direction, respectively. We

consider a half-filled system ($N/2$ particles on the N -site system) and exclude the double occupancy. The ground state and low energy states of this model are shown in Figure 6 [25]; at $V > V'$ a unique ground state with a so-called checkerboard type of charge ordering takes place. At higher energy level, there is a bunch of macroscopically degenerate excited states, so-called three-sublattice state and its contingents, which go down and join the ground state at $V = V'$. Let us briefly explain the origin of their degeneracy using Figure 7(a); first, divide the lattice points into three sublattices (A, B, C), and color them by black, white, and gray, where black and white are the filled and empty sites, respectively. Next, draw a hexagon along the black and white sites, and we may find that the energy of this hexagonal unit is unchanged by taking the center gray site to be either black or white. This already gives a $2^{N/3}$ fold degeneracy. Now, take another hexagon edged by gray and white sites, and turn all the three grays black. Then, one could again flip the black inside to white, which costs no energy. This game could generate numerous contingent states of the same energy one by one, which is the origin of the macroscopic degeneracy.

Figure 6. Low energy structure of the classical Ising model, $E_{\text{ising}} = \sum_{ij} V_{ij} n_i n_j$, (subtracting the constant term, $(-2V + V')N/4$ from Equation (3)), on the anisotropic triangular lattice as a function of V with $(V' + V)$ -fixed. Three different characteristic states (chain stripe, three-sublattice and contingent states, checkerboard stripe) are the ground state at $V' \geq V$, $V = V'$, and $V' \leq V$, respectively. The low energy excited state is classified by the number of “defects”(red vertical bonds with $\bullet\text{-}\bullet$ or $\circ\text{-}\circ$), N_d , which has the same number for all different chains. The energy of these states increases as $N_d(V' - V)/2$.

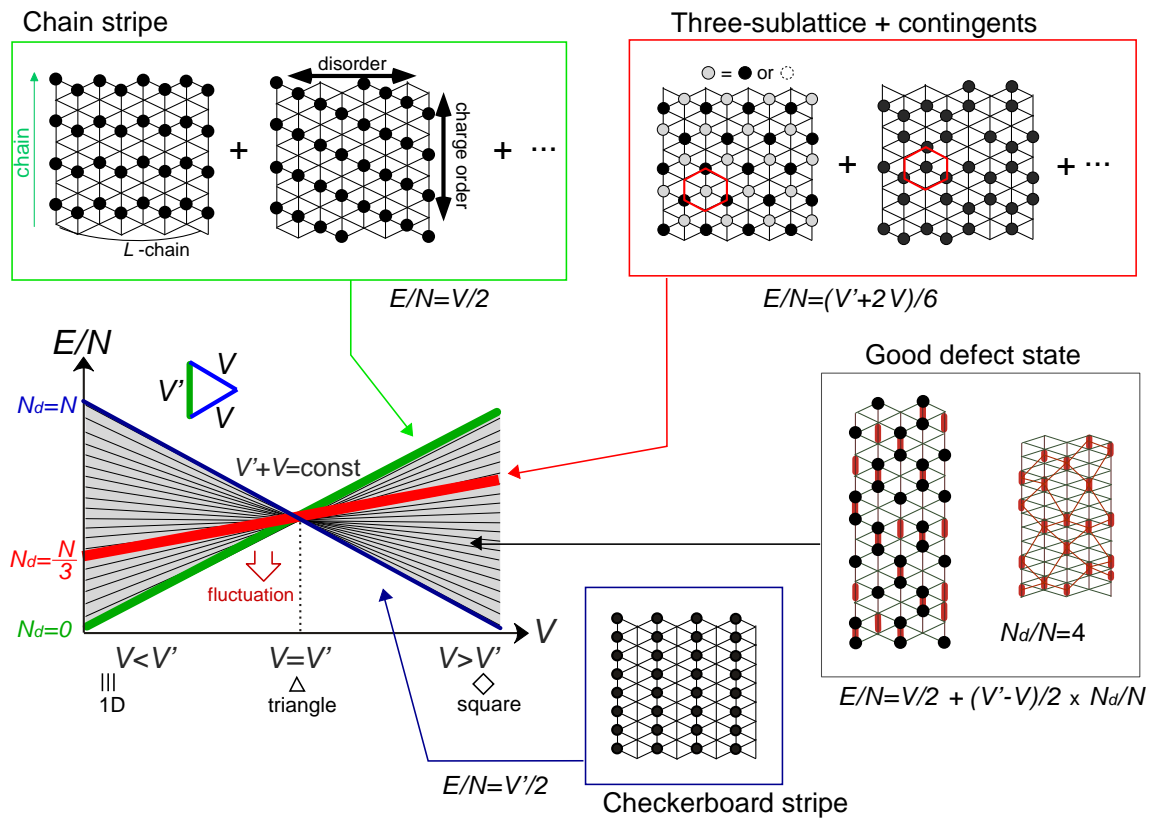


Figure 7. Energetics of the classical Ising model (Equation (3)) on the anisotropic triangular lattice. (a) Hexagonal unit of the three-sublattice state (ABC), and three adjacent hexagons. Flipping the center of the hexagon from black to white does not change the energy, and this operation generates numerous contingent states; (b) Energy diagram of the unit plaquette at $V' > V$. The plaquettes of the excited energy $(V' - V)/2$ form a series of low energy “good defect” states classified by the defect number N_d/N , as shown in Figure 6.

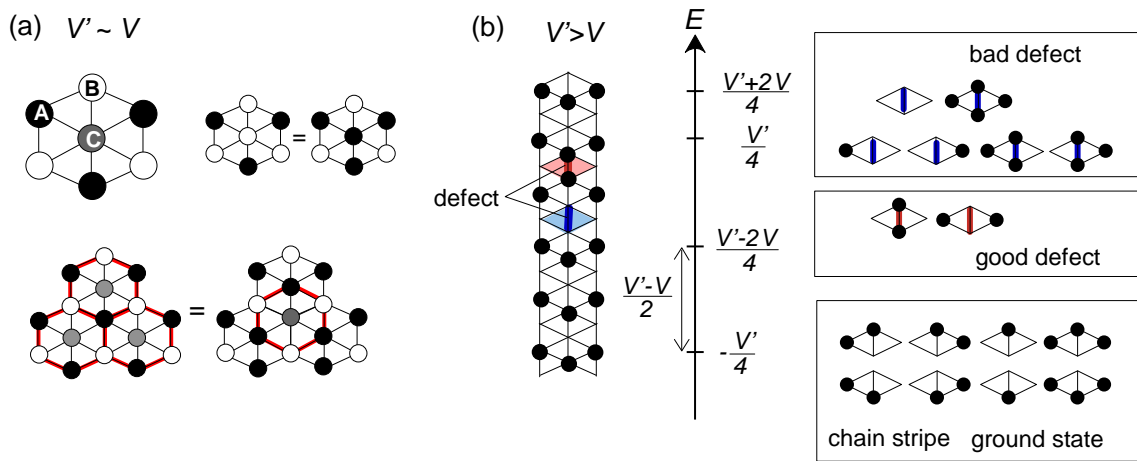
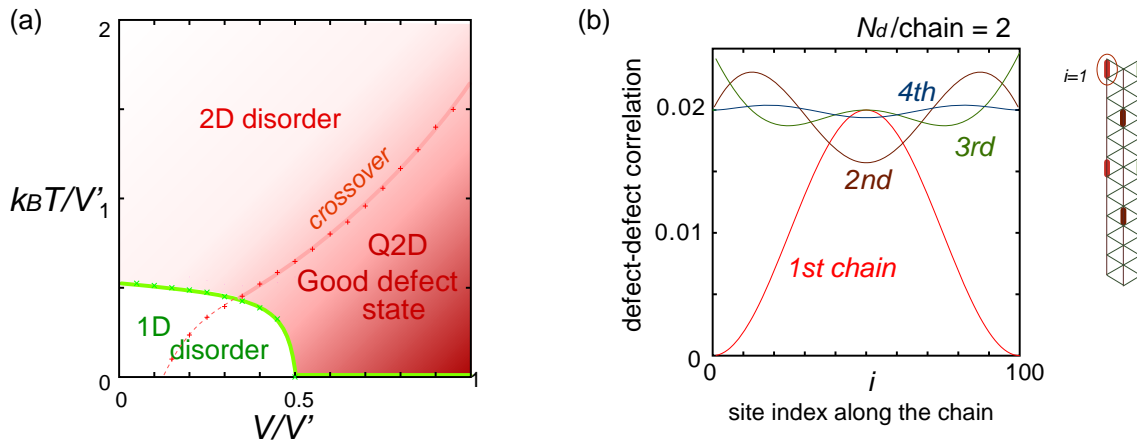


Figure 8. (a) Finite temperature phase diagram of the classical Ising model on an anisotropic triangular lattice at $V' > V$ [26] and (b) the defect-defect correlation function with one defect fixed to site $i = 1$ of the first chain [26].



Another series of degenerate states are found on the other side of the axis, $V' > V$, which we call chain stripes. This time, strong V' forms a charge order along each vertical chain, but there still is a choice of taking their phases as either $\circ \bullet \circ \bullet \dots$ or $\bullet \circ \bullet \circ \dots$. Both choices are energetically degenerate, since the two diagonal V -bonds are still frustrated. These remaining degrees of freedom multiplied over L -chains contribute to the 2^L fold degeneracy.

Still, the classical story does not end until we refer to the other series of the degenerate excited states which form dense energy levels, in between the three-sublattice group and the chain-stripe group. We start from one of the chain stripe ground states, and introduce a “defect” into a charge order, *i.e.*, $\bullet \bullet$ or $\circ \circ$ bond along the chain. The energy loss of introducing the defects can be evaluated in unit of

a plaquette, shown in Figure 7(b); there are sixteen plaquettes, eight of which are elements of chain stripes, two with a lowest excitation energy are called “good defect”, and the other six “bad defects” have higher excitation energy. The plaquettes share bonds/sites with their neighbors and are thus not freely chosen, *i.e.*, random insertion of defects always includes both good and bad ones. One then needs a rule to exclude “bad defects” and form excited states with only “good defects”; it is to introduce them alternatively between the nearest neighbor chain, as shown in Figure 6 (see [26] for details). This means that the number of “good defects” per chain N_d/L is the same for all chains, and the energy levels are discretized linear to N_d/N . It is interesting to find that the above mentioned chain stripe, three sublattice, and checkerboard stripes all belong to the “good defect state” and are classified by the number of these “good defects” exactly as zero-defect state, $N/3$ -defect state, and N -defect state, respectively.

Hotta *et al.* found an “order by disorder” reconstruction of such classical energy levels by the thermal fluctuation [26]. The state with larger degeneracy, namely larger entropy S , will gain more free energy, $F = E - TS$ (see Figure 5(b)) at finite temperature. The phase diagram of Equation (3) on the anisotropic triangular lattice calculated by the classical Monte Carlo method is shown in Figure 8(a); the “good defect state” covers the low temperature and frustrated region. This is because each of the good defect state manifold with fixed $0 < N_d < N/3$ has higher entropy than the classical chain stripe ground state. The defects fluctuate along the chain but keep their alternating configuration, which looks like a soft lattice structure in the charge ordered sea; the defect-defect correlation function in Figure 8(b) shows that the defects form equally spaced lattices on a thermal average with relatively small amplitude of spacial modulation.

The second example of “order by disorder” is the one driven by the quantum fluctuation, $t/V > 0$. Consider the tV -model, and start from its strong coupling classical Ising limit ($t = 0$). The lowest order of t mixes the three-sublattice and its contingent states within their own manifold (Figures 6, 7(a)), makes them dispersive, and lifts their massive degeneracy. The other stripe manifolds have smaller quantum energy gain of order t^2 , thus at $V \sim V'$, the three-sublattice manifolds overtake the stripes and form a unique ground state. This strong coupling picture is verified by the numerical calculations, as briefly summarized in the following. The phase diagram of the t - V model shown in Figure 9(a) is obtained by the density matrix renormalization group calculation (DMRG) on a $N = 8 \times 6$ cluster [27], one of the most established numerical methods in low dimension which could efficiently include the quantum fluctuation from short to long range. The above mentioned state that we named “a pinball liquid” [28], which originates from the three-sublattice and contingent states, is sandwiched between the two stripes. The reconstruction of energy levels by t is obvious in Figure 9(b); the energies of the two stripes and three-sublattice states are lowered by $\propto t^2$ and t and exhibit two crossing points as first order transitions. Figure 9(c) shows the spacial distribution of charges along one bond direction; when one enters the pinball liquid phase, a three-fold poor-rich-rich (pin-ball-ball) distribution of charges develops. The fermions (holes) at the center of the hexagon form a solid, and the itinerancy of fermions develops along their edges, which could be approximately regarded as a spontaneous spacial phase separation into solid and liquid components. The energetics roughly explains why this happens (see Figure 9(d)); if one tries to move the “pins” to its vacant neighbor, the energy loss is $2V$, thus they cannot easily move. In contrast, moving the “balls” along the vacant honeycomb lattice has no classical energy cost but instead brings a kinetic (quantum) energy gain. The long range order of the solid component is verified by the size scaling

analyses on the charge structural factor by a variational Monte Carlo (VMC) method [29,30]. The VMC calculation also showed that the Fermi surface reconstruction takes place at the phase transition from a normal metal to a pinball liquid. As shown in Figure 9(e), the momentum distribution function, $n(k)$, is a step function at $V = 0$, which gives the round Fermi surface (electron pocket). At large V , $n(k)$ exhibits a fine structure, and by folding the Brillouin zone into one-third, another stepwise function appears, forming a round hole pocket. This indicates a Fermi liquid nature of the balls. These results support a picture that the solids partially melt and form quasi-particles(balls) which are almost free despite their highly correlated origin. We note that there is still a possibility of having quantum liquid state originating from the good defect manifolds ($0 < N_d < N/3$ in Figure 6), in between the horizontal stripe and the pinball liquid, but the examination on this issue needs calculations on larger lattice size, and is left for future study.

Nishimoto and Hotta analyzed the t'/t -dependence of a charge gap of the horizontal stripe ordering at $V' > V$ [27], and found that the nature of the gap changes from the weak coupling ones (charge-density-wave) to the strong coupling (charge order) ones at around $V' \sim 3t$. This fact is consistent with the features of the phase boundary in Figure 9(a); the boundaries between stripe and the pinball liquid extending straight up toward the strong coupling limit start to deviate from the linear slope at around $V \sim V' \lesssim 3t - 4t$. Thus, this value is a crossover boundary between the weak and strong coupling regime. In this way, the strong coupling physics could be applied to a wide parameter region in the quarter-filled electronic systems.

Does the inclusion of the spin degrees of freedom blur the above exotic solid-liquid picture? This question, not simple enough, is later on studied by Cano-Cortes *et al.* [31] in the extended Hubbard model at 3/4-filling, which approximately correspond to taking $U \ll \infty$ from the tV -results and allow the double occupancy of electrons. Before discussing this issue, we overview the earlier works on the same extended Hubbard model, which are summarized in the phase diagram in Figure 10(a); the results of the exact diagonalization by Merino *et al.* [32], VMC by Watanabe *et al.* [33], and DMRG with by Nishimoto *et al.* [34] are put together for comparison. The one by Merino *et al.* [32] was the first work to point out the possibility of frustration in organic systems, while they missed the existence of three-fold metallic state, whose period is incompatible with the shape and size of their cluster ($N = 4 \times 4$). Otherwise, the results by different methods are overall qualitatively in agreement with each other. However, large quantitative discrepancies of the phase boundaries indicate the extreme difficulty of dealing with the correlation effects in frustrated systems in the intermediate coupling region[35], as we discussed in Section 2.3. Actually, the mean field result on the same model by Kaneko and Ogata [36] has a pseudo-degenerate energy level (degenerate within the order of $\sim \mathcal{O}(10^{-3}t \sim 10^{-4}t)$) in the metallic state at the center of the phase diagram, consisting of many different stripes and three-fold states (“metal (competing)” in Figure 10(a)). Although the VMC calculation may lift some of the pseudo-degeneracy by including the correlation effect, the energies of the two stripes and three-fold state are still almost degenerate within the range of $10^{-4}t$ [33].

Figure 9. Numerical results of the t - V model on the anisotropic triangular lattice. (a) Phase diagram at $t = t'$ by the DMRG with $N = 8 \times 6$ [27]; (b) Energy along the fixed value of $V + V'$ obtained by the exact diagonalization with $N = 6 \times 4$ [28], showing the reconstruction of levels from those of the classical limit (Figure 6). The kink of the energy line gives the phase boundary shown in (a) [25]; (c) Charge distribution function $\langle n_i \rangle$ along one bond direction by the DMRG, from [27]; (d) Sketch of a pinball liquid state (left) and the process of moving pins (right panel); (e) Momentum distribution function $n(k)$ of the full Brillouin zone (left panel), and of the folded ($1/3$) Brillouin zone (right panel) by the VMC in [29], together with the schematic Fermi surfaces. The axis k is taken along the arrow of the Brillouin zone in the inset. At $V/t = 24$, $n(k)$ is shown for full and $1/3$ -folded Brillouin zones, and the latter displays a reconstruction of the Fermi surface, with a Fermi liquid type of discontinuity.

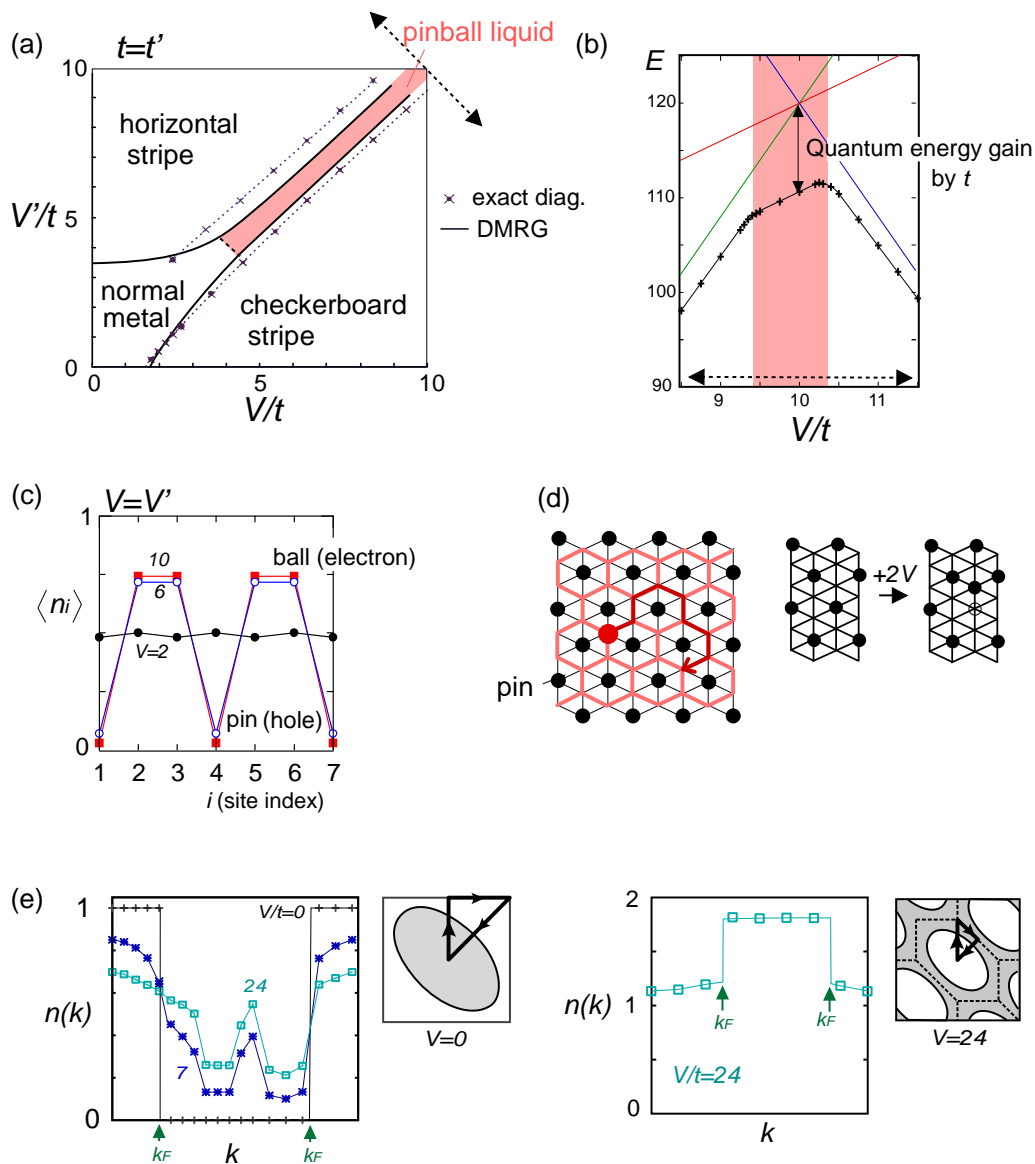


Figure 10. Numerical results of the 3/4-filled extended Hubbard model on the anisotropic triangular lattice. (a) Phase diagrams obtained by the exact diagonalization ($N = 4 \times 4$, Merino *et al.*) [32], VMC ($N \sim 400$, Watanabe *et al.*) [33], and DMRG ($N = 8 \times 6$, Nishimoto *et al.*) [34], put together on the plane of V and V' with $U/t = 10$ and $t' = 0$. Adapted with permission, copyrighted by the American Physical Society ([32,34]) and the Physical Society of Japan ([33]); (b) Single-particle spectrum $A(k, \omega)$ by the exact diagonalization and (c) double occupancy of the charge-rich sublattice at $V = V'$ (DMRG), adapted with permission from [34], copyrighted by the American Physical Society.

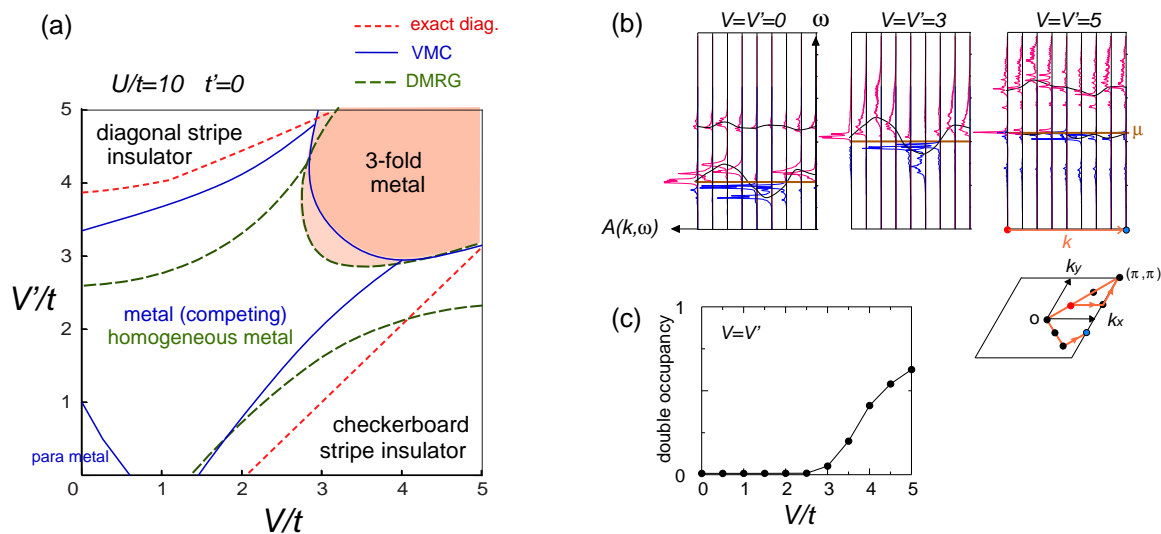
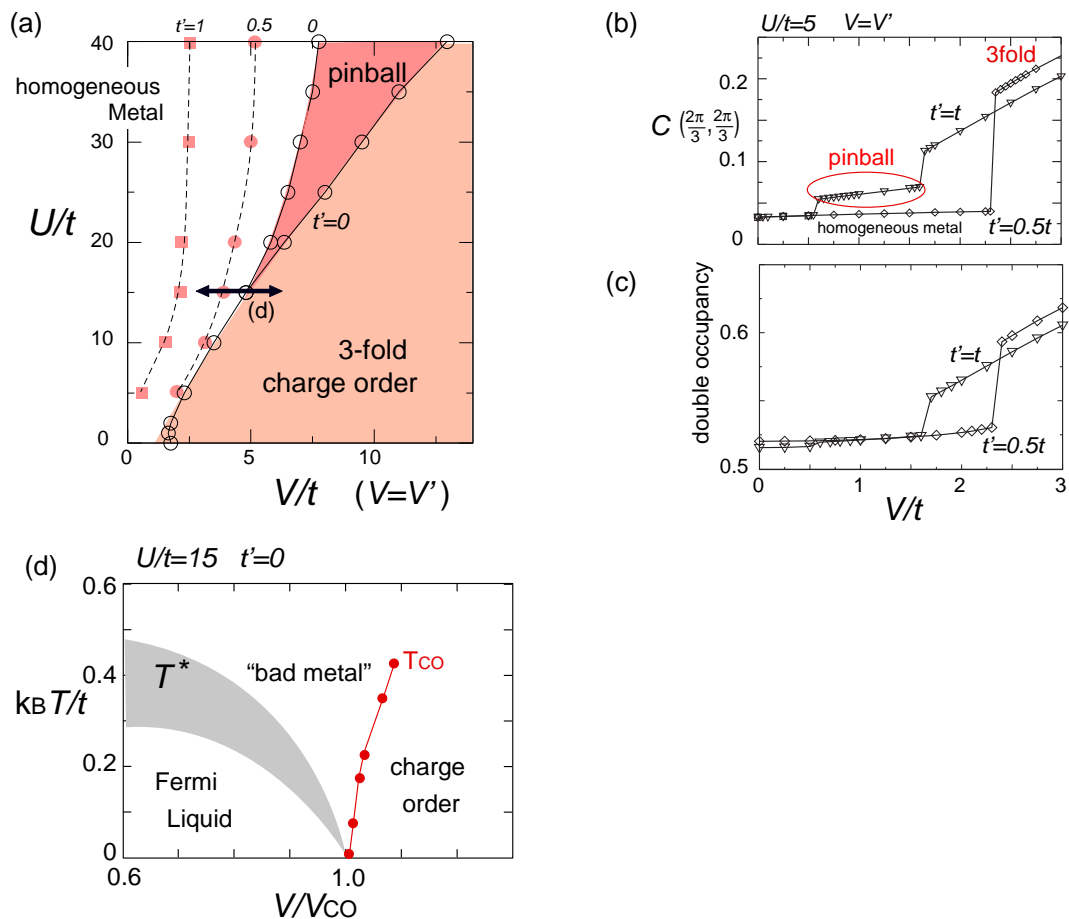


Figure 10(b,c) shows a single-particle spectrum (an energy dispersion including the many-body effect), $A(k, \omega)$, and the double occupancy of charges by Nishimoto *et al.* [34]. As the interaction increases to $V = V' \sim 5$, a very narrow band characterizing a heavy effective mass is found near the Fermi level [37]. There, the double occupancy amounts to $d \sim 0.66$, namely ($d_A = d_B \sim 1$ and $d_C \sim 0$). This means that the number of holes in the A and B sublattices responsible for the conduction is strongly suppressed, which is consistent with the narrow band width.

The latest exact diagonalization study by Cano-Cortes *et al.* [31,38] finally concluded that the above three-fold charge ordered metallic state *is not necessarily identified* as a pinball liquid. As found in their phase diagram in Figure 11(a), the three-fold charge ordered state at smaller U and large V , which is identical to the one in Figure 10(a), is transformed to a pinball liquid state at larger U . The two are discriminated by the charge structural factor, $C(2\pi/3, 2\pi/3) \sim n^2$ and $n^2/3$ with $n = N_e/N$, and by the different degree of double occupancy, d , shown in Figure 11(b,c). At large V with $d \sim 0.66$, the three sublattices form an almost closed shell, $n_A = n_B = 2$ and $n_C = 1$, ($d_A = d_B = 1$ and $d_C = 0$) and the holes in A and B are depleted. The results are in good agreement with the one by DMRG in Figure 10(c). With increasing U/V , part of the hole density spills out from the C sublattice, and becomes a separate fluid moving freely along A and B, with the distribution of $n_A = n_B = 7/4$ and $n_C = 1/2$ in terms of charge density. The fact that only one-third of the charges participate in the ordering is detected as plateaus in $C(2\pi/3, 2\pi/3) \sim n^2/3 = 0.08$. The boundary between the two, $U/V \sim 3$, simply follows the counting of energies regarding U and V with the above two sets of charge densities. In this way, the

relation of the extended Hubbard and t - V phase diagrams are made clearer. If one takes larger U/t from those of Figure 10(a), the pinball liquid replaces the three-fold metal, and their phase boundaries with stripes become straight as in Figure 9(a). The three-fold charge order and a pinball liquid have different amount of charge distribution, but share the same spacial symmetry. Thus, it is not clear whether the two are separated by the second order transition or a crossover [39], which is a difficult issue to be concluded solely by the numerics.

Figure 11. Numerical results of the 3/4-filled extended Hubbard model on the anisotropic triangular lattice, by Cano-Cortes *et al.* using exact diagonalization with $N = 12$ and 18. (a) U/t - V/t phase diagram; (b) Charge structural factor ($C(k)$) and (c) double occupancy against $V = V'$ at $t' = 0$. In the non-interacting limit, $d = (n/2)^2 = (0.75/2)^2 = 0.5625$, which increases to 0.66 in the three-fold state. $C(\pi/3, \pi/3) \sim n^2/3$ and n^2 for the pinball and the three-fold charge order, respectively; (d) Finite temperature phase diagram along the bold arrows in (a) ($U/t = 15, t' = 0$). Adapted with permission from [31,38], copyrighted by the American Physical Society.



There still remains some intriguing issues on the homogeneous metallic state in the weaker coupling region of the phase diagram, Figure 11(a). The double occupancy of hole carriers is almost completely depleted as, $d_h = (1 - n_\uparrow)(1 - n_\downarrow) = 1 - d - 1.5 \sim 0$, with $d \sim 0.5$ (Figure 11(c)). The volume fraction available for each hole carrier is thus significantly reduced. At finite temperature, this somewhat localized Fermi liquid crosses over to a “bad metal” [38]. Cano-Cortes *et al.* evaluated the crossover

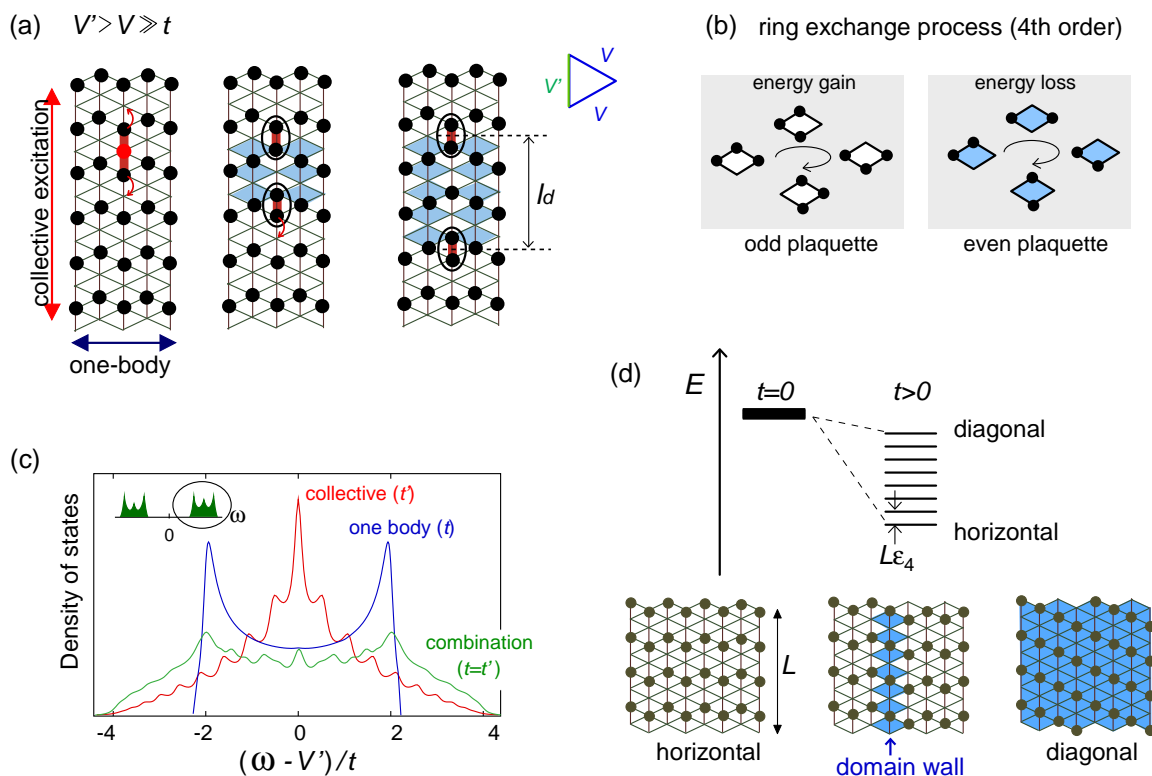
temperature T^* , as shown in Figure 11(d); the specific heat coefficient shows a peak at T^* , and above this temperature, the kinetic energy starts to deviate from those of the Fermi liquid. The suppression of T^* with increasing V might be ascribed to the quantum criticality [39,40], namely, the enhanced charge order fluctuations in approaching the phase boundary could easily destroy the coherence of a Fermi liquid. Another possible scenario related to Wigner-Mott localization is studied on the charge ordered metallic state forming a narrow phase between the charge ordered insulator and a homogeneous metal [41]. Like the metals close to the Mott transition, an incoherent metal could be stabilized above T^* , in which the electrons partially behave as fluctuating magnetic moments on a charge rich site, and partially behave as itinerant carriers [39]. Below T^* , the coherence grows and the state becomes a Fermi liquid. In any case, the role of frustration, $V = V'$, on this matter is not yet clarified. However, if one takes $V' = 0$ in Figure 11(a), the homogeneous metal should become a charge ordered insulator, thus the geometrical frustration at least works to expand the strongly correlated metallic region.

3.2. Frustrated Metal: Excitations

The excited states of the frustrated systems include as much rich physics as their ground states. Back to the Ising model in Figure 6, the $V' > V$ region still has a semi-macroscopically degenerate low energy manifold. Due to this residual frustration, doping a single particle can yield a many body excited spectrum. The DMRG calculation [34] on the extended Hubbard model indeed points out that the one-particle excitation spectra at $V' > V$ contains a strong charge fluctuation at low energy in the chain direction associated with the classical degeneracy. Again, forget about the spins and take a look at the sketch of classical stripe state with one particle added, shown in Figure 12(a) [42]. This doping corresponds to inserting two defects, as $\bullet \bullet \bullet$. By shifting one charge on the top/bottom of these three adjacent particles upward/downward, the defects separate in the chain direction as $\bullet\bullet$ and $\bullet\bullet$, without the classical energy loss. The defect pair is the analogy of a kink and an anti-kink or a pair of domain walls realized in the one-dimensional antiferromagnetically ordered spin chain, and in the purely one-dimensional charge ordered systems as well [43,44]. Since each of them carry $e/2$ charge, the description of “fractional charges” may also be adopted. The inclusion of t to this classical limit will mix a series of two-defect states. Note that each of the particles on the top/bottom of upper/lower defects can hop only one site upward/downward, but the successive hopping of many particles will carry defects further. Therefore, this propagation has a many-body character [42].

Now, if we include a higher order perturbation, the separation of defects increases the energy linear to the distance, l_d . The reason is simple; the plaquette which includes even number of particles has higher energy than the one with the odd number of particles by ϵ_4 , by the fourth order ring exchange process on a plaquette, shown schematically in Figure 12(b). As the defects separate, the plaquettes between them are replaced from odd to even ones, and the “potential energy” increases by $2l_d\epsilon_4$. This is called a “confinement effect”. One could visualize it as a string connecting the two defects with a very small but finite tension. The defects are loosely bound by a string, and form a nearly continuum but have discrete levels reflecting a typical length scale of defects. Note here that the defects are regarded as pure fractional charges only when they are deconfined (zero tension). Otherwise, the defect pair is forming a quasi-particle with large spacial coherence.

Figure 12. (a) Sketch of spinless particles in the strong coupling regime of the anisotropic triangular lattice t - V model at $V' > V$. Doping one particle to a stripe ($N_e = N/2 + 1$) generates two $\bullet\bullet$ which separate by distance l_d due to the successive hopping of many particles; (b) Ring exchange processes on a plaquette with odd/even numbers of particles gain/lose the energy; (c) Many body density of states ($\sum_k A(k, \omega)$) of this collective excitation (t') together with the one-body excitation (t) along the stripe [42]; (d) Energy levels of the chain stripe manifolds at $V' > V \gg t$, which have the domain wall excitation. The diagonal/horizontal stripe filled with even/odd plaquettes has the highest/lowest energy.

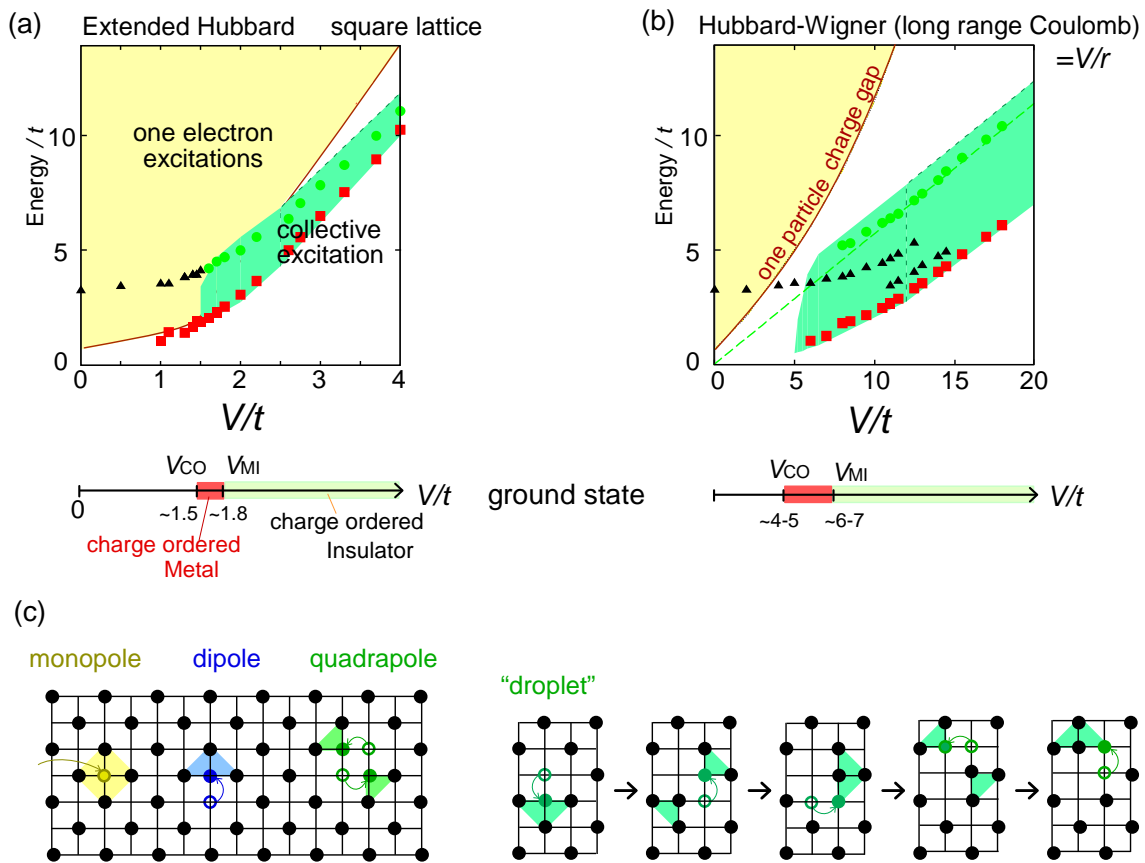


When the doped particle propagates along the stripes with no classical energy cost, none of the above particular features appear. It just behaves as a one-dimensional free particle. Thus, at $V' > V$, the doping causes two different types of dispersion along the vertical (t') and horizontal (t) direction, which Hotta and Pollmann call a “ $1\oplus 1$ dimensional metal” [42]. Indeed, the density of states of for t and t' shown in Figure 12(c) are completely different. When both t and t' are finite, the combination of the two is realized. In contrast, if one dopes a particle on the checkerboard stripe at $V > V'$ we only find a free one-dimensional type of density of states with a van Hove singularity at the band edges.

Besides the above charged excitation, the neutral excitations have the collective nature. Again, recall the 2^L -degeneracy of the half-filled spinless system in the classical limit (Figure 6) and see how it is lifted by t . The degeneracy remains up to third order, thus the plaquette ring exchange process is required. Let us start from a horizontal stripe filled with odd plaquette in Figure 12(d). Now, shift the phase of the horizontal charge order of one chain (exchange empty and filled sites), which replaces the L -odd plaquettes along this chain with even ones, costing the energy of $dE = L\epsilon_4$. The same operation generates the equally spaced (dE) energy levels, and the horizontal stripe with maximum number of odd

plaquette is selected as a ground state. The excitations here are regarded as inserting a domain-wall one by one. The same kind of neutral excitation is present even if we include the spin degrees of freedom in the charge ordered state of the extended Hubbard model at $V' > V$. This time, however, the diagonal stripe is energetically favored against the horizontal stripe by the second order spin exchange couplings [45], and become a unique ground state (Figure 10(a)).

Figure 13. Excitation spectra of (a) the extended Hubbard model and (b) the Hubbard–Wigner model $V_{ij} = V/|r_i - r_j|$, both on a square lattice. Adapted with permission from [46]. Copyrighted by the American Physical Society. The ground states of the two models are shown in the lower panels; (c) Sketch of excitations from the checkerboard charge ordered ground state of the square lattice; monopole (one-electron excitation) by the doping of a particle, and the neutral dipole (bound state of exciton, *i.e.*, electron and hole) and quadrupole (bound state of two excitons) excitations [46]. The “droplet” is a many-body excitation in (b), which propagates by the resonance between the dipole and the quadrupole at the lowest order of t .



While this review is focused on the anisotropic triangular lattice, there are other cases providing the physics of frustration. One example can be found on a square lattice ($V' = 0$). Dynamical mean-field theory (DMFT) [41,47] and the exact diagonalization [48] show that the extended Hubbard model at quarter-filling exhibits a charge ordered metallic phase—a Fermi liquid state, but with considerably large degree of charge disproportionation breaking the translational symmetry—in a very narrow range ($\sim O(t/10)$) in the vicinity of the insulating phase. This metallic state itself is not directly related to

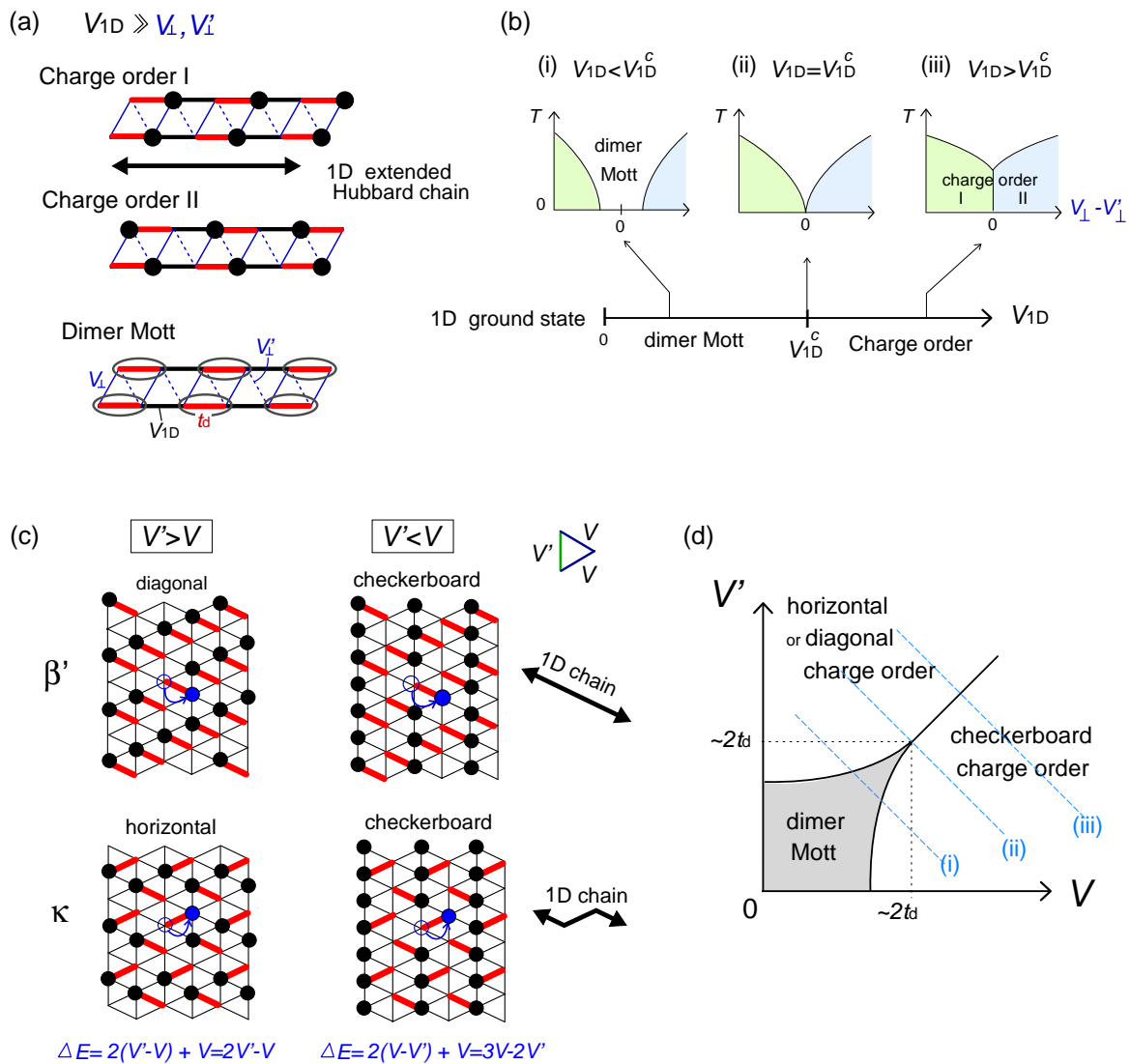
the frustration effect. However, replacing the nearest neighbor V_{ij} 's in the extended Hubbard model to longer range Coulomb interaction, $V_{ij} = V_0/|r_i - r_j|$ (Hubbard–Wigner model), extends this metallic phase significantly [46]. The frustration effect of the long range interactions is visible in their excitations. Figure 13(a,b) shows the excitation spectra of the extended Hubbard and Hubbard–Wigner models. In the Hubbard–Wigner model, the low-lying collective excitation occurs well below the one-particle charge gap, even at $V \leq V_{\text{MI}}$, which is generally expected to happen only in the strong coupling insulators. The origin of this unusual collective excitation is depicted in Figure 8(d). Besides the charged (monopole) excitation, there are two neutral excitations, dipole and quadrupole, which shift one and two particles, respectively, to the neighboring sites from the ground state configuration. When the long range Coulomb interaction is present, the electrostatic energy is essentially insensitive to local details, since it is mostly determined by the long-range tails of the Coulomb potential. Therefore, the dipole and quadrupole excitations have comparable energies, and could mix. Thus, the combination of two triangles in the quadrupole, called “droplet”, propagate by resonating between the dipolar and quadrupolar configurations (we show example in Figure 13(c)). Such motion gains a kinetic energy of order t and a low-energy continuum is formed. This is one of the examples in electronic systems showing that, in order to have frustration, we do not necessarily have to stick to the particular geometry of a lattice.

3.3. Dielectrics

Experimental studies started to reveal that many organic crystals are potential dielectrics, insulators which respond to the external electric field. Here, we particularly have in mind the spontaneous polarization of electric moment, ferroelectricity and antiferroelectricity. The realization of “electronic ferroelectricity”, which is the one not driven by the ionic displacement of the lattices but originates from the modification of the electronic wave function, is actually discussed in the context of charge ordering in one of the charge transfer salts [49]. In the charge ordered state without bond ordering (namely all bonds are equivalent), the ferroelectricity is absent. To have ferroelectricity, a finite degree of inequivalency of bonds in the unit cell is needed [50], which is often present in the organic crystals by construction. Here, a possible emergence of ferroelectric phases related to frustration effect are discussed.

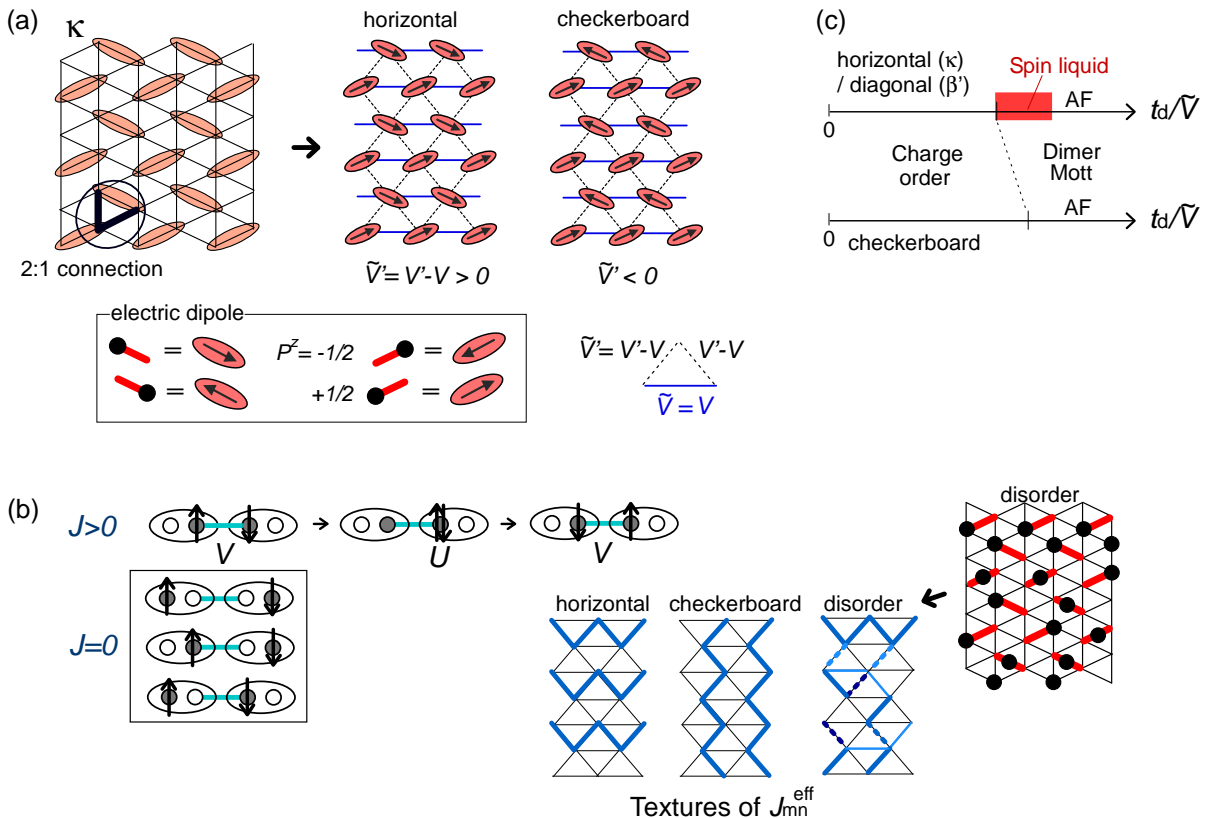
Yoshioka *et al.* studied the one-dimensional quarter-filled extended Hubbard model interacting with the neighboring chains via small V_{\perp} - and V'_{\perp} -bonds, using the bosonization technique combined with the inter-chain mean-field (see Figure 14(a)) [51]. To understand their context we draw schematic phase diagrams in Figure 14(b); when U and t_d are enough large, the ground states in one-dimension ($V_{\perp} = V'_{\perp} = 0$) are divided into the charge order and the dimer Mott insulator by the intra-chain Coulomb interaction at $V_{1D} = V_{1D}^c$ [52]. The small inter-chain Coulomb interactions, V_{\perp} and V'_{\perp} ($\ll V_{1D}$), basically stabilize the charge ordering. Thus, as far as $V_{1D} \geq V_{1D}^c$, the system is charge ordered for all values of V_{\perp} and V'_{\perp} (case (iii)). At $V_{1D} < V_{1D}^c$, there is a critical value of $|V_{\perp} - V'_{\perp}|$ to have a charge order (case (i)). This is because V_{\perp} and V'_{\perp} work as mean-field potentials onto a neighboring chain along the two edges of the triangular unit, and if the charges are ordered, the signs of the two potentials differ and cancel out. This could be regarded as a “weak frustration effect”.

Figure 14. (a) Schematic illustration of the one-dimensional dimerized ($t_d > t$) extended Hubbard chain interacting with U and V_{1D} and coupled to neighboring chain via V_{\perp} and V'_{\perp} ; (b) Schematic phase diagrams of model (a) on the plane of temperature (T) and $V_{\perp} - V'_{\perp}$, which Hotta constructed referring to the renormalization group and inter-chain mean-field results by Yoshioka *et al.* [51]. The ground state of the pure 1D chain for $U \gg V_{1D}$ is shown in the lower panel. Depending on the relative strength of V_{1D} against V_{1D}^c , the finite temperature phase diagram at finite $V_{\perp} - V'_{\perp}$ is classified into three cases; (c) Dimerized (t_d in bold red bonds) β' - and κ -type of lattice structures based on the anisotropic triangular lattice with V and V' . The classical degeneracy of charge order at $V' > V$ (chain stripe in Figure 6) is lifted and the diagonal(β') and horizontal(κ) stripes, which maximally gain the energy by $\epsilon_2 N/2$, become the unique ground states; (d) Schematic ground state phase diagram of the dimerized extended Hubbard model on the lattices (c) at $U \gg t_d \gg t$, which Hotta depicted by regarding diagonal (β') and horizontal (κ) bond directions as 1D chain.



We now extend the discussions to the two-dimensional dimerized lattices, e.g., so-called β' and κ -type geometry shown in Figure 14(c). The starting point is again the classical spinless Ising particle system without t 's. The ground states at $V' > V$ and $V' < V$ are the degenerate chain stripe and the unique checkerboard stripe, respectively (see Figure 6). By turning on $t_d > 0$ while keeping other t_{ij} zero (or small enough), one could specify the one-dimensional dimerized chains running along the V -bonds, coupled to the neighboring chain via V and V' , i.e., $(V_{1D}, V_{\perp}, V'_{\perp}) \sim (V, V, V')$. However, the above quasi-one-dimensional result do not straightforwardly apply when $V_{1D} \sim V_{\perp}$. The energetics will clarify this issue— moving one particle in the stripe states to the neighboring site by t_d costs a classical energy of $\Delta E = 2|V' - V| - V$. When $\Delta E \gtrsim t_d$, this local quantum fluctuation gives only a small energy correction, $\epsilon_2 = 2t_d^2/\Delta E$, and the stripe order remains as a ground state. Figure 14(c) shows the horizontal, diagonal and checkerboard stripes, which form a ground state in the β' and κ -type crystals at $V' \neq V$. In contrast, in the opposite limit, $t_d \gg \Delta E$, the particles resonate within each dimer almost freely, and all stripe configurations connected by this fluctuation mix and form a dimer Mott insulator. Thus, the competition between t_d and ΔE rules the phase transition between the two insulators. We could thus draw a schematic phase diagram in two dimension shown in Figure 14(d). The frustration effect stabilizes the dimer Mott phase at $V \sim V'$, where ΔE takes a minimum.

Figure 15. (a) Mapping of κ -type site-based lattice into a dimer-based anisotropic triangular lattice; (b) Configuration of charges on two adjacent dimers which have finite/zero exchange coupling J , and the texture of J_{mn}^{eff} for ordered and disordered charge configurations; (c) Schematic phase diagram of the dipole-spin model [20].



Hotta proposed a transverse Ising model (Equation (6)) on an effective lattice in unit of dimers to study the above issue directly [20]. This model is understood by introducing the transverse field, t_d , to the classical Ising model (see Figure 3). This time, the Ising degrees of freedom, $P_m = \pm 1/2$, is an electric dipole, representing the site location of charge in the m -th dimer (*i.e.*, different from the particle number $n_i = 0, 1$ of the Ising model in Equation (3)). Mappings of the site-based lattices to the dimer-based ones are shown in Figure 15(a). The dimers form another anisotropic triangular lattice consisting of \tilde{V}_{mn} -bonds and their anisotropy reflects the geometry of the original lattice. When dimers have the 2:1 site connections via two bonds V and V' , the competing $V \sim V'$ suppress the interactions between dipoles as, $\tilde{V}_{mn} = V' - V$. This weak frustration effect is a source of the dimer Mott insulator near $V = V' \sim 2t_d$, as we just discussed. Then, depending on the sign of $\tilde{V}_{mn} = V' - V$, either the horizontal or the checkerboard type of dipolar solid (charge order) is stabilized as in Figure 14(d).

The correlated nature of dipoles influence the magnetic property, which is studied by combining the above transverse Ising terms with the Kugel–Khomskii-type of term (Equation (7)), which we call the dipole-spin model [20]. They are obtained by the perturbation up to second order from the $U \gtrsim V_d = \infty$ -limit of the extended Hubbard model (Section 2.2). At the first order, the transverse Ising term determines the ground state of the charge sector (dipole), and at the second order, the Kugel–Khomskii term rules the spin degrees of freedom through the couplings with the dipoles. The spin exchange interaction is evaluated from the coefficients of $S_m \cdot S_n$ in Equation (7) as,

$$J_{mn}^{\text{eff}} = W_0 - W_z P_m^z P_n^z + W_{xy} \frac{1}{2} (P_m^+ + P_m^- + P_n^+ + P_n^-) \quad (9)$$

To consider its origin, focus on two sites belonging to different dimers connected by a single bond, as shown in Figure 15(b). If the two are filled with up and down spins, respectively, the charge can hop to another dimer, forming doubly occupied site with excited energy $U - V$, and then comes back, which yields a finite Heisenberg exchange, $J = W_z = 4t^2/(U - V)$. However, if either of these sites are empty, the exchange process is absent. Therefore, the antiferroelectric alignment, $P_m^z P_n^z < 0$, enhances J_{mn}^{eff} , as is seen from the second term in Equation (9). When the adjacent dimers have 2:1 site connections, the linear combination, $W_z = J' - J$, is adopted. (For more details including other terms, see [20]). This rule enables the construction of the spacial texture of J_{mn}^{eff} on a lattice for any given charge (dipole) configuration. The geometry of J_{mn}^{eff} the localized spins on dimers recognize is thus far from being isotropic, e.g., those shown in Figure 15(b). In the vicinity of the phase transition from a dimer Mott to charge ordering, the correlation of dipoles develops, and the timescales of the fluctuation of short range charge orders slow down. The net J_{mn}^{eff} produced by the “nearly frozen” dipoles on dimers shall be inhomogeneous, and resultantly, a quantum disorder of spins emerges [20]. Such a dirty “spin liquid” could possibly emerge near the phase transition into the horizontal/diagonal charge ordering in which the frustration effect is relevant, but hardly near the checkerboard stripes (see Figure 15(c)).

3.4. Spin Liquid Mott Insulator

A quantum disordered “spin-liquid” state breaking no global spin or lattice symmetries has been pursued ever since Anderson proposed an exotic resonating valence bond liquid of spin singlets [53]. From its incipency, an antiferromagnetic quantum spin systems on a regular triangular lattice was

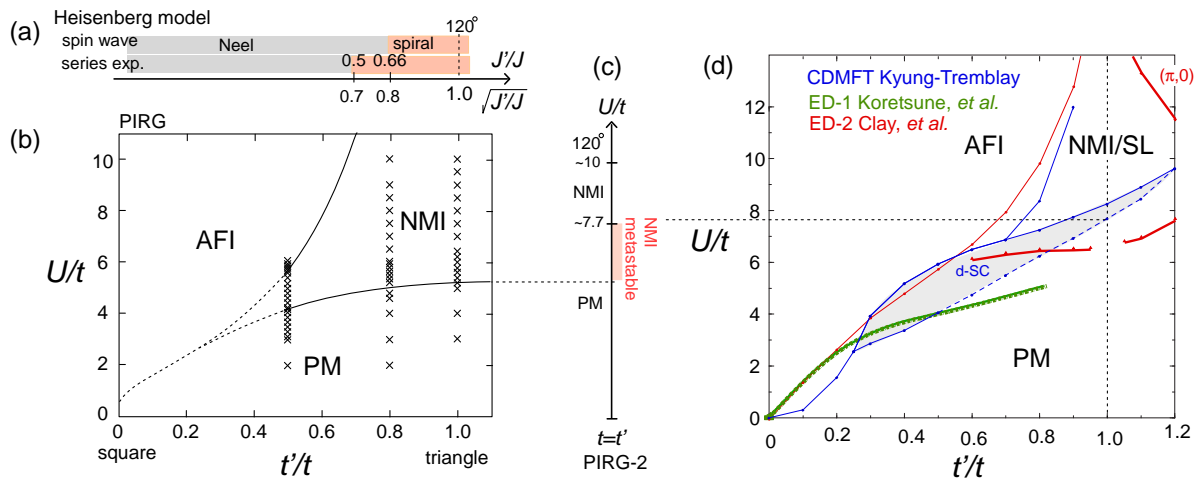
the potential candidate, with an expectation that the geometrical frustration effect of nearest-neighbor Heisenberg exchange interactions, J , destabilizes an ordinary Néel order. However, its ground state turned out to be a 120° -type of Néel order [54,55]. When introducing an anisotropy of exchange interaction along one bond direction of the triangle, J' , weakened toward the square lattice, the 120° -order turns into a spiral order by gradually modifying its wave number, and finally a Néel order sets in. The schematic phase diagrams based on the results by the spin wave theory [56] and series expansion [57] are shown in Figure 16(a). Later on, Misguich *et al.* found that the inclusion of the ring exchange process of four spins on the plaquette yields a liquid state, suppressing a spin gap at $J_4 \gtrsim J/4$, where J_4 is the ring-exchange coupling constant [58]. Since the value of J_4 in the localized spin system is generally considered to be weaker by the orders of magnitude than this critical value, a more realistic model was in need.

A breakthrough was brought by the inclusion of the charge degrees of freedom. Morita *et al.* proposed a phase diagram of the single-band Hubbard model on the anisotropic triangular lattice at half-filling shown in Figure 16(b) by the path integral renormalization group (PIRG) calculation [59]. A nonmagnetic insulating phase (NMI) spreads over a wide region of anisotropy of the transfer integral $t'/t \gtrsim 0.6$. A series of studies followed, based on several other numerical methods, which are partially summarized in Figure 16(c,d). Koretsune *et al.* gave an exact diagonalization study on several different clusters up to $N = 18$, and averaged the results over the twisted boundary conditions to minimize the size/boundary effect [60]. Kyung and Tremblay applied a cellular dynamical mean-field theory (CDMFT) with 2×2 cluster embedded in bath sites, and proposed a superconducting phase just below the Mott insulator [61]. Clay *et al.*, by the exact diagonalization on a $N = 4 \times 4$ lattice, reported a $(\pi, 0)$ -magnetic ordering at large U region, and claimed an absence of superconductivity [62]. Another PIRG study [63] with $N = 36$ argued that in the regular triangle $t = t'$, the 120° order in the Heisenberg model appears at $U/t \gtrsim 9.2$ via first order transition from NMI.

The current consensus here could at least arrive at the presence of three phases, where NMI exists over a relatively wide region, $t'/t \gtrsim 0.5$ and $U/t \gtrsim 4$ between the AFI and the PM phases. The transition point from PM to NMI should lie between $U/t \sim 4-5$ at $t'/t \sim 0.5$ to $6-8$ at $t' \lesssim t \sim 1$. Let us briefly point out three main unsettled issues.

$d_{x^2-y^2}$ -wave superconductivity (d -SC); Kino and Kontani first studied the t'/t -dependence of d -SC by the fluctuation exchange (FLEX) approximation [64]. The variational Monte Carlo (VMC) studies [65,66] report a robust d -SC at the same intermediate range, $t'/t \sim 0.4-0.7$, which is in qualitative agreement with Kyung and Tremblay's CDMFT (Figure 16(d) have d -SC at lower U than the above two studies). Dayal, Clay, and Mazumdar deny the d -SC phase, both by the exact diagonalization (red lines in Figure 16(d)) and by the QP (quantum number projection)-PIRG [67]. In general, the characteristic energy scale of SC should be several orders of magnitude smaller than t . The small cluster size of $N \sim \mathcal{O}(10)$ which leads to the artificial discretization of energy levels larger than that order may not be enough to stabilize the SC phases. The exact diagonalization or QP-PIRG of $N = 4 \times 4$ to 8×8 might thus underestimate the stability of SC. Contrarily, FLEX, CDMFT and VMC basically have a mean-field character, somewhat lacking the long range correlation, in which case the SC shall be overestimated. For these reasons, the degree of stability of the d -SC phase cannot be easily concluded.

Figure 16. (a) Ground state of the antiferromagnetic Heisenberg model on an anisotropic lattice with $J'/J \sim (t'/t)^2$. The phase boundary between the Néel and the spiral orders by the spin wave theory [56] and by the series expansion [57] are separately shown; (b)–(d) Phase diagrams of the single-band Hubbard model on an anisotropic triangular lattice at half-filling; (b) PIRG by Morita *et al.* with $N = 14 \times 14$ (300 basis) [59]; (c) PIRG-2 by Yoshioka *et al.* at $t' = t$ ($N = 6 \times 6$ with 500 basis) in [63]; (d) CDMFT by Kyung and Tremblay (with d -SC phase) [61], where solid/broken lines indicate the first/second order phase transition, and the exact diagonalizations made by Koretsune *et al.* (ED-1) [60] and by Clay *et al.* (ED-2, no d -SC phase) [62]. Besides the ED-1 line showing the onset of a charge gap, Koretsune *et al.* calculated two extra lines (not shown here), indicating the magnetic phase transition and the disappearance of Drude weight. The latter Drude line at larger U/t may merge to the present ED-1 line in the bulk limit. Adapted with permission, copyrighted by the Physical Society of Japan (PIRG,ED-1) and by American Physical Society (CDMFT,ED-2).



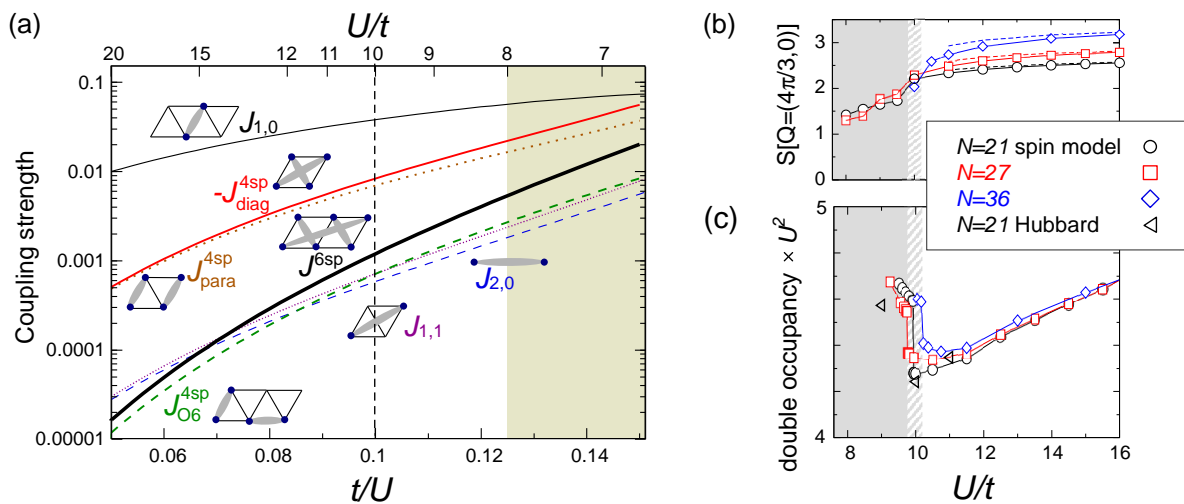
Order of transition; the transition from PM to AFI/NMI at $t'/t < 1$ is basically of first order, observed by the jump in the physical quantities such as double occupancy. The magnitude of jump decreases with increasing t'/t toward unity [59,60,62] (for the first order transition from SC to NMI, see [68]). At $t'/t = 1$, Morita *et al.* [59] argues the continuous transition at $U_c \sim 5.2t$. Later on, Yoshioka *et al.* showed that $U_c \leq U \leq U_{c1} \sim 7.4t$ could be considered as a coexistent region of PM and NMI, and the NMI which starts to emerge at $U \geq U_c$ remains as a metastable state until U_{c1} , at which point a true first order transition takes place.

Other magnetic phases; it is in overall agreement that at larger U/t region of NMI, there should be a transition to another magnetic phase. Which kind of spacial texture appears— 120° degrees ($t = t'$ by Yoshioka *et al.* (PIRG-2) [63]), stripes or other wave vectors (Clay *et al.* (ED-2) [62], Mizusaki and Imada [69] (QP-PIRG))—still depends on methods or on analyses.

Yang *et al.* elucidated the origin of such unconventional NMI phase by the strong coupling approach [70], performing the exact diagonalization on the effective model derived by the perturbative continuous unitary transformations (PCUT). This PCUT, a perturbation from the $U = \infty$ limit (free spins) up to twelfth order, derives an extremely complicated spin model, which includes the effect of charge fluctuations as multiple and long range spin exchange terms among up to six-spins. A parameter

range down to $U/t \sim 7$, *i.e.*, until the very vicinity of the metal-insulator transition, is studied on a regular triangle ($t' = t$). Here are their main conclusions. Among numerous exchange terms, the most important correction to the conventional Heisenberg model ($J_{1,0}$) is the four-spin interactions on a diamond plaquette ($J_{\text{diag}}^{4\text{sp}}$), and the higher-order contributions become by orders of magnitudes smaller (see Figure 17(a)). The ratio, $J_{\text{diag}}^{4\text{sp}}/J_{1,0}$, at $U/t \lesssim 10$ is indeed enough to stabilize the gapless spin liquid. The structural factor of the 120° order, $S(Q = (4\pi/3, 0))$, drops at $U/t \sim 10$, as shown in Figure 17(b), suggesting a transition into a “spin liquid” phase. Above/below $U/t = 10$, $S(Q)$ is enhanced/unchanged with the system size N , indicating that the magnetic long range order is only present above this critical point. At $U/t < 10$, one could expect either a short range correlation or a critical algebraic decay of correlation functions. A jump in the double occupancy is observed as a consequence of the level crossing of the ground state energies (see Figure 17(c)), in agreement with those calculated for the Hubbard model at $N = 21$. This work succeeded in showing that the low-energy effective model in the insulating phase, even in the vicinity of the metal-insulator transition, is indeed a pure spin model—in other words, they confirmed that the strong coupling perturbation theory is extended down to the order of $t/U \sim \mathcal{O}(0.1)$. This result strongly supports the first proposal on the origin of a spin liquid state by PIRG [59], that the spacial charge fluctuation near the Mott transition plays crucial role.

Figure 17. Numerical results by Yang *et al.* adapted with permission from [70], copyrighted by the American Physical Society. (a) Coupling constants of the multiple spin exchange processes by PCUT. Broken line at $U/t \sim 10$ indicates a Mott transition; (b) Structural factor and (c) the double occupancy of the effective spin model by PCUT to compare with those of the original half-filled Hubbard model by the exact diagonalization.



Still, the detailed nature of the NMI remains unclear. The QP-PIRG study indicates an unconventional magnetically gapless state, consisting of degenerate states with different wave numbers and different total spins [69], whereas the comparable model calculation to confirm even a presence/absence of a spin gap is still severely lacking, and it is thus a difficult issue to be fully concluded. Clarifying the nature of low energy excitations of the two dimensional microscopic models is indeed a difficult task. There exists instead a considerable amount of literatures devoted to the phenomenological low-energy effective

theories on quantum spin liquids, proposing several elementary excitations of the exotic particles coupled to gauge fields [71]. They are the attempts to reconcile with the experimental measurements on low-temperature thermodynamic properties, e.g., those of the organic κ -ET or dmit salts [72]. However, the direct connections of their ideas to the microscopic models are still far from being achieved — there are some, but very few attempts, e.g., Motrunich interpolated the picture of a spinon Fermi surface with the Heisenberg spin models including ring exchanges [73]— thus they lie outside the scope of the present review.

4. Weak Coupling Regime

The amount of theoretical works dedicated to the organic material systems over the past ten years are the approaches to the extended Hubbard model sometimes including the electron-lattice terms from a weak-coupling point of view. Their two main issues should be (1) How the shape of the Fermi surface, or the energy dispersions near the Fermi level, is deformed by the inclusion of Coulomb interactions, and (2) How the electron-lattice coupling modify the electronic states. The deformation of the Fermi surface has been discussed in Hubbard models in the context of high- T_c superconductors [74]; a strong antiferromagnetic spin fluctuation develops near the antiferromagnetic phase transition and modifies the Fermi surface so as to improve the nesting condition around the particular wave number. In analogy, a strong charge fluctuation which develops near the charge ordering transition may play a similar role. The electron-lattice coupling basically serves as a driving force of the reconstruction of the Fermi surface toward the $2k_F$ -charge density wave state. However, the raw (non-interacting) $2k_F$ -nesting instability is weak in two dimension, thus such coupling plays a secondary role to choose from one of the quasi-one-dimensional (stripe) or three-fold charge orders, the one which has the most compatible “nesting” vector.

The weak coupling approach starts from the non-interacting band and treats the interaction effect perturbatively. The static charge susceptibility in the random phase approximation (RPA) is given in the form,

$$\chi_c(q) = \frac{\chi(q)}{1 + W(q)\chi(q)}, \quad W(q) = U + V(q) + D(q) \quad (10)$$

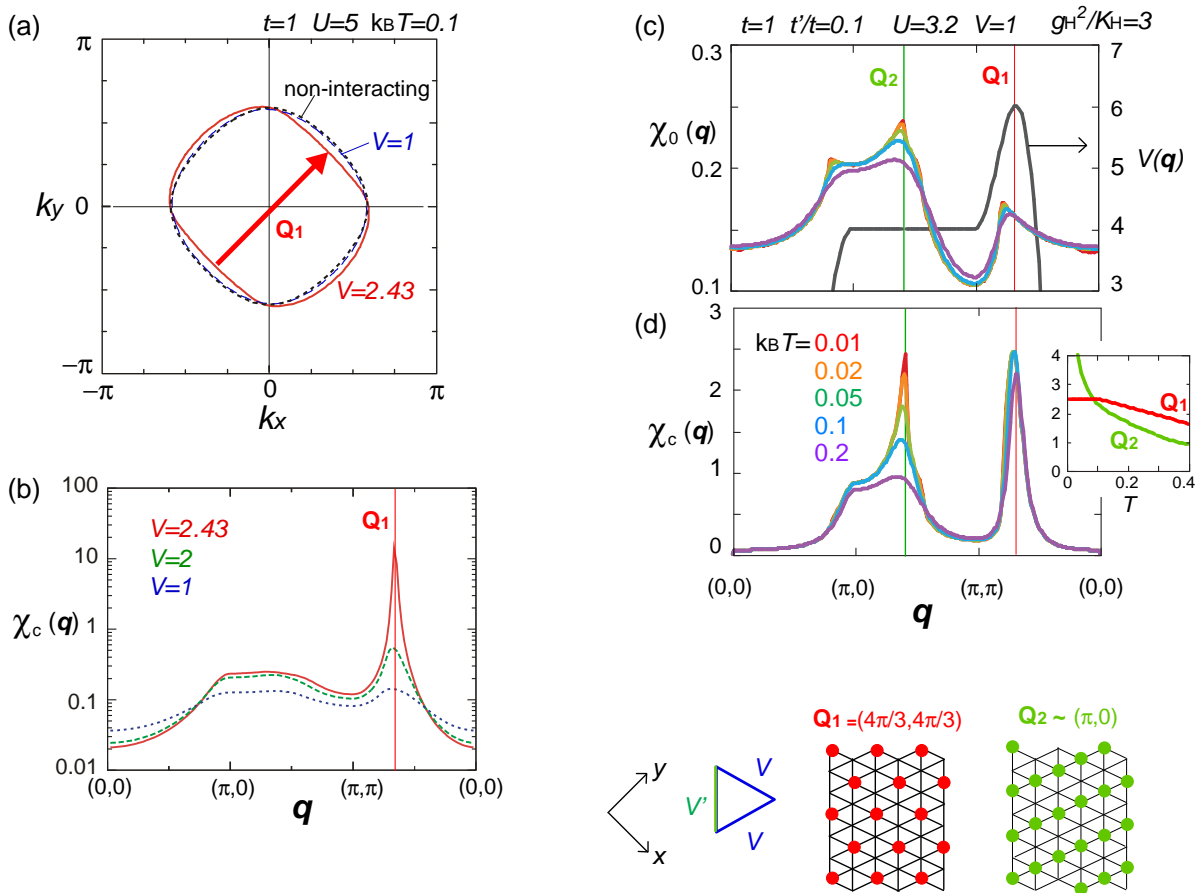
where $V(q)$ is the Fourier transform of V_{ij} , and the Green’s function of the phonons $D(q)$ is included in $W(q)$. The enhancement of the charge susceptibility is detected by the vanishing of the denominator, $1 + W(q)\chi(q) \sim 0$, thus how $W(q)$ and $\chi(q)$ behave under the given Fermi surface and by the interaction effects is examined. In the RPA, a bare susceptibility (reflecting the structure of the non-interacting Fermi surface), $\chi_0(q) = 1/\sqrt{N} \sum_k (f(\epsilon_{k+q}) - f(\epsilon_k))/(\epsilon_k - \epsilon_{k+q})$, is adopted as $\chi(q)$.

In contrast, in the fluctuation exchange (FLEX) approximation, $\chi(q) = \int G(k+q)G(k)$, is obtained from the full one-particle Greens’s function $G(k)$ including the self-energy term, $\Sigma(k)$. The effect of charge fluctuation that modifies the self energy (or equivalently the Fermi surface) through the exchange interaction, $\tilde{V}(q) = V(q)/(1 + V(q)\chi(q))$, is then taken into account by determining these quantities self-consistently. Such effect not included in RPA is visible in $\chi_c(q)$ by FLEX through the modification of $\chi(q)$ from the bare $\chi_0(q)$. Now, the self-consistent Hartree–Fock approximation could also include the modification of the self energy through the effective transfer integral, \tilde{t}_{ij} , via the Fock terms.

However, without the feedback of higher order fluctuation effects to $\Sigma(k)$, it is insufficient to discuss the modification of Fermi surface [75].

Yoshimi *et al.* studied the extended Hubbard model without the electron-lattice coupling by the FLEX approximation [75]. As shown in Figure 18(a) a non-interacting Fermi surface of a square-lattice- t ($t' = 0$) at quarter filling has a round shape unfavorable for nesting, *i.e.*, for the divergence of $\chi_0(q)$ at some q . Due to the interaction, $V = V'$, its shape is then modified toward a rectangle, and at $V = V_c$, $\chi_c(q)$ diverges due to the vanishing of the denominator at a wave vector, Q_1 , as can be seen from a growth of peak in Figure 18(b). This Q_1 characterizes the three-fold charge ordering, which is basically the one discussed in the context of charge frustration in Section 3.1. In a weak coupling language, one may say that $V(q)$ conforms the Fermi surfaces to drive the system into a charge order.

Figure 18. (a) Fermi surface and (b) the static charge susceptibility, $\chi_c(q)$, of the extended Hubbard model at $V = V'$, $U/t = 5$ and $t' = 0$ obtained by the FLEX calculation. Adapted with permission from [75], copyrighted by the Physical Society of Japan. The charge order sets in at $V/t \sim 2.5$ for this choice of parameter; (c) χ_0 and $\chi_c(q)$ of the extended Hubbard model plus the Holstein type of electron-lattice coupling (characterized by $g_H^2/K_H = 3$), obtained by the RPA calculation. Adapted with permission from [76], copyrighted by the American Physical Society. The lower panels indicate the charge ordering pattern corresponding to the Q_1 and Q_2 wave numbers.



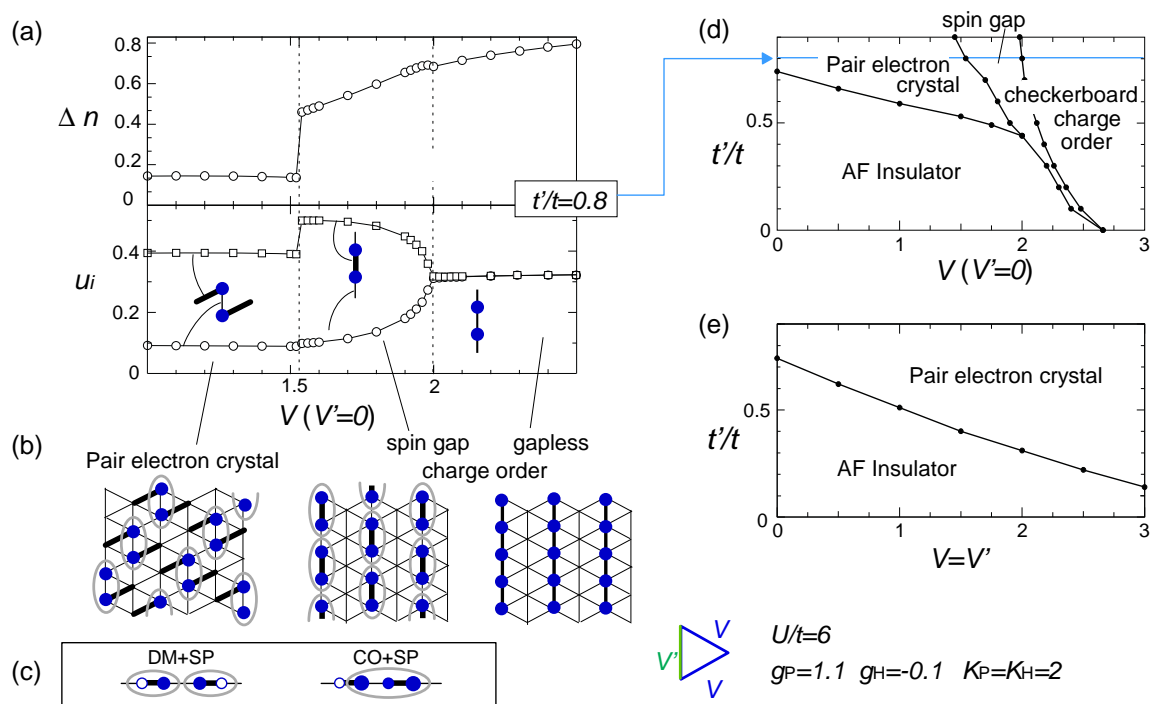
The electron-lattice coupling aids the instability at the other wave vector, Q_2 , to compete with Q_1 . Udagawa and Motome studied the electron-lattice coupling effect to the extended Hubbard model by the RPA [76]. This method sacrifices the above mentioned charge fluctuation effect and may underestimate the instability at Q_1 , but could deal with the competition between the two energy scales in a simpler manner (see Figure 18(c,d)); the $\chi_c(Q_1)$ -peak with no doubt originates from the $V(Q_1)$ -peak, which reflects the spacial geometry of V 's. In contrast, the $\chi_c(Q_2)$ -peak is due to a bare nesting instability in $\chi_0(q)$ and measures the tendency toward the stripe charge ordering. A rough comparison with the results by Yoshimi *et al.* tells us that $\chi_c(Q_2)$ is significantly enhanced, and this could be ascribed to the electron-lattice coupling, g_H (Equation (8)), through the $W(Q_2)$ -term in Equation (10).

Recall that the ground state of the extended Hubbard model is a diagonal stripe (Q_2) or a checkerboard stripe charge order (see Figure 10(a)), whereas in the related experiments on θ -ET₂X, the horizontal stripe pattern is dominant [77] (see Section 5.1). To explain the experiments, Tanaka and Yonemitsu carried out a mean-field study to search for a possibility of having the horizontal stripe with the aid of the electron-lattice coupling [45]. They examined several different Peierls-types (g_P) of lattice modulations, and found one Peierls coupling which stabilizes the horizontal stripe charge order at $V' > V$ against all the other orderings; it increases/decreases the t_{ij} along charge rich/poor horizontal stripe. Accordingly, the exchange coupling of spin chains ($\propto t^2$) effectively formed along these stripes is enhanced, and the resultant energy gain works as an advantage to stabilize the horizontal charge ordering. They consider that such rather unusual modulation comes from the rotation of the molecules. Once $g_P > 0$, this modulation is stable even in the three-fold charge ordered state, in which the texture of charges show coexistence of two periods [78]. The coexisting two orders in the mean-field level shall turn into the above competing short range charge fluctuation at Q_1 and Q_2 , when the electronic correlation is taken into account.

An interplay of spins with charges and bonds is pursued in the exact diagonalization study by Dayal *et al.* on the extended Hubbard model with both Holstein- and Peierls-type of electron-lattice couplings on the anisotropic triangular lattice [79]. They proposed a state called “pair-electron crystal”, out of a freezing of bonds and charges simultaneously with a spin-Peierls singlet formation. The degree of charge disproportionation Δn and lattice displacement u_i are shown in Figure 19(a). The pair-electron crystal has moderate degrees of Δn and u_i , compared to those of the charge ordered state at larger V . One of the sites forming charge and bond-orders ($\circ=\bullet$) create extra singlet pairs with its neighboring analogue as $\circ=\bullet-\bullet=\circ$ by the exchange interaction ($\propto t^2$) along the vertical bond (“-”), as shown in Figure 19(b). This state could be identified as the one referred to as DM + SP (dimer Mott-spin Peierls state) reported in the quantum Monte Carlo study by Otsuka *et al.* [80], and is discriminated from the spin gapped charge order which we roughly make correspondence with the CO + SP (charge ordered-spin Peierls state) (see Figure 19(c)). The phase diagram at $V' = 0$ (square lattice- V) in Figure 19(d) is consistent with those of Otsuka *et al.*; the pair-electron crystal (DM + SP) turns into the spin gapped charge order (CO + SP) with increasing V , and finally a normal charge order without lattice distortion ($u_i = 0$) sets in. Dayal *et al.* further showed in Figure 19(e) that the geometrical frustration, $V = V'$, completely replaces the charge ordered phases with the pair-electron crystal. To understand this result, recall our discussions in Section 3.3—the geometrical frustration in V destabilized the charge order against the dimer Mott insulator. The similar picture shall apply here by regarding the pair-electron crystal as an analogue of

the dimer Mott insulator. However, compared to the pure dimer Mott case, the pair-electron crystal is more significantly stabilized, possibly owing to the spin degrees of freedom or to the spontaneous lattice modulation instead of the intrinsic dimerization. The increasing degrees of freedom thus could cope much better to release the frustration of V .

Figure 19. Exact diagonalization results by Dayal *et al.* [79] on the quarter-filled extended Hubbard plus the Holstein and Peierls-model for $N = 4 \times 4$ anisotropic triangular lattice with $U/t=6$, $g_P=1.1$ (square type along V -bonds), $g_H=0.1$, and $K_P=K_H=2$. (a) Charge disproportionation $\Delta n = n_i - 0.5$ and the degree of lattice modulation u_i at $V' = 0$ (square lattice) as functions of V (along $t'/t = 0.8$ in (d)); (b) Pair-electron crystal and charge orders with and without spin gap; (c) DM + SP and CO + SP states studied by Otsuka *et al.* [80] to be compared with the pair electron crystal and the spin-gapped charge order; (d,e) Comparison of phase diagrams of square- V ($V' = 0$) and triangular- $V = V'$ on the planes of V and t'/t ; (a,d,e) adapted with permission from [79], copyrighted by the American Physical Society.



5. Experimental Findings

Most of the theories we went through so far have been motivated by the experimental studies on two families of organic crystals, θ -(BEDT-TTF) $_2X$ and κ -(BEDT-TTF) $_2X$ (BEDT-TTF = bis(ethylenedithio)tetrathiafulvalene is abbreviated as ET, and X stands for the monovalent anions with closed shell), whose stacking layers provide a quasi-two-dimensional electronic system spanned on a lattice of ET molecules with three-quarter filling of electrons. They have brought into the world the two states of matter, charge order and dimer Mott insulator, now representing the field [7]. Meanwhile, a relatively high symmetry of their crystal structure are bringing in new phases related to the frustration

effect. As we saw in Figure 2(a), the lattice structures of θ - and κ -types are ideal triangles with anisotropy of bonds along only one of the three directions, if we take a molecule and a dimerized molecule as a unit of a lattice, respectively. Here, it is beyond our scope to discuss more than a recent fragment of the amounts of experiments given on these two families. We refer the interested reader to the recent articles [81,82].

5.1. Competing Orders

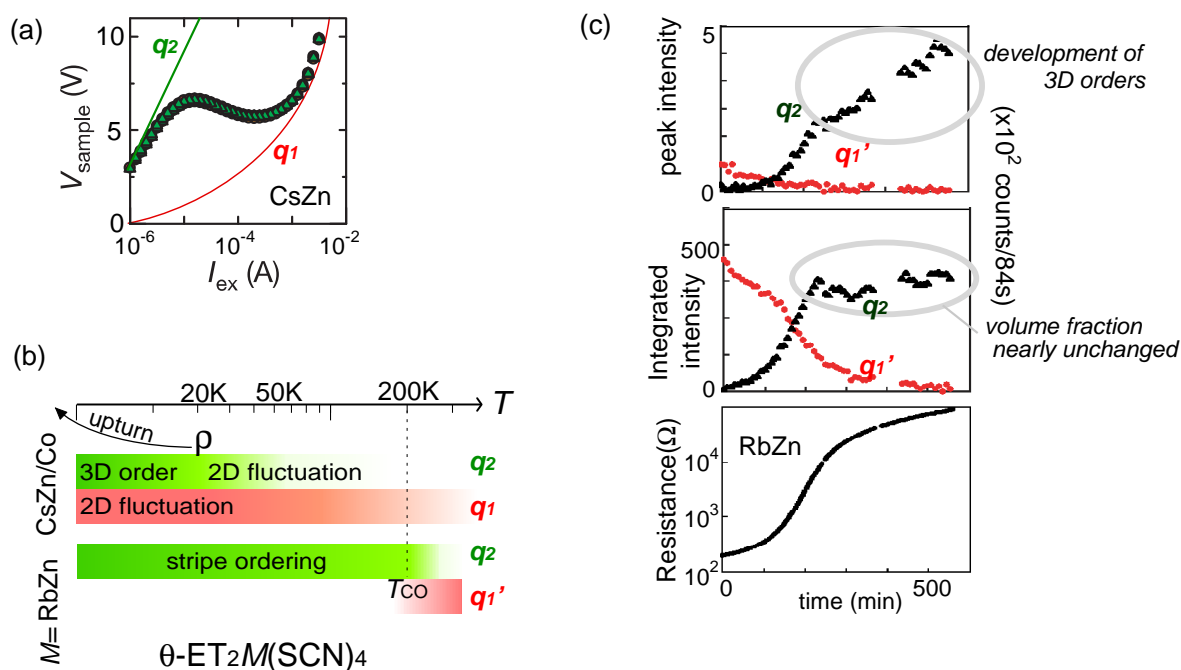
What triggered increasing interests on frustration effect in organic crystals was a story of an “organic thyristor” in θ -ET₂CsZn(SCN)₄—a nonlinear conductance characterized by the downturn of resistivity near the onset of the I-V curve [83]. The coexisting two distinct short range correlations of a nanometer scale, indicated by $q_1 = (2/3, k, 1/3)$ and $q_2 = (0, k, 1/2)$ -diffuse rods in the X-ray diffraction (k is the arbitrary inter-layer wave number), was recognized as an experimental evidence of inhomogeneity under a competition of two orders. The sign of such inhomogeneity was already detected by the broadening of the linewidths in the earlier C¹³-NMR measurement [84]. By decomposing the I-V curve into two components, one can ascribe them to the relatively metallic and insulating states, as shown in Figure 20(a). The activation charge gap and the q_2 -X-ray intensity both show the linearly decreasing behavior against the current density, identifying the origin of the I-V characteristics [85]. Indeed, it is now an overall consensus that the q_1 -peak is related to the three-fold charge ordered metallic state and the q_2 -peak to the insulating horizontal stripe charge order (for corresponding theories, see Section 4). However, it is not obvious how such inhomogeneity emerges in a clean bulk crystal almost free from impurities. The open issues are, (1) Are the two short range orders separate in space ?, namely, either forming any domain or coexisting in a single phase; (2) Could the temperature-dependent behavior of I-V characteristics really be explained ?; (3) How could the details of q_1, q_2, q'_1 be explained in a consistent/unified manner? ; (4) What is the most important energy scale, and is it due to disorders or related to phonons ?

The answer to (1) is given by the experiment [86], which carried out simultaneously the diffraction and resistivity measurements on an isostructural material, θ -ET₂RbZn(SCN)₄. This salt displays intrinsically the same competition but at a higher temperature and with somewhat different $q'_1 = (1/3, k, 1/4)$. The overall features of the low energy properties of RbZn-salt in comparison with CsZn-salt are summarized in Figure 20(b). The time evolution of the integrated intensity of the RbZn-salt in Figure 20(c) shows that the q'_1, q_2 -volumes are exclusive, namely separating in space. The growth of the size of the q_2 -domain (see the peak intensity) was detected by the rods of the X-ray; it develops along the interlayer direction—*not within the two-dimensional plane*—without changing its total volume, and is responsible for the increase of the resistivity.

Theories must rather be responsible for the remaining issues. Regarding (2), the static nonequilibrium mean-field theories confirm that the horizontal stripe order is taken over by the three-fold charge order under the applied electric field as well as at higher temperature; Yukawa and Ogata dealt with the extended Hubbard model without lattice distortions, and showed that the solid component of the three-fold charge order partially melts by the electric field, but the phase itself is stabilized thermodynamically against the horizontal charge ordering [87]. Tanaka and Yonemitsu included the

electron-lattice coupling and found that the lattice distortion in the “coexistent state” of three-fold and stripe charge orders (in mean-field theory) drops suddenly at a critical electric field, wiping out the horizontal stripe component, and enhancing the electric current [78]. This drop is reminiscent of a non-linear response of the inter-layer conductivity (along which the horizontal stripe domain extends) at low electric field [88].

Figure 20. (a) IV characteristics of θ -ET₂CsZn(SCN)₄, adapted with permission from [83]; (b) Low temperature characters of the q_1 , q'_1 and q_2 peaks of CsZn/Co and RbZn salts; (c) Time evolution of the X-ray intensities (peak and integrated ones) measured simultaneously with the resistivity, adapted with permission from [86], copyrighted by the Physical Society of Japan.



Kuroki [89] made an attempt to explain the material-dependent wave numbers q_1 and q'_1 (issue (3)) on the RPA basis, by introducing several extra V_{ij} 's between those separated by two molecular spacing. He showed that the peak positions of the charge susceptibility $\chi_c(q)$, which directly reflects the geometry of $V(q)$ through $W(q)$ in Equation (10), is sensitive in the chain direction, which reminds us of the degeneracy of chain stripes in the strong coupling theory. We shall put in mind that trying to fully reconcile the wave numbers in experiments with theoretical results without any other colloquials are sometimes tenuous, since the increasing number of the model parameters makes the equations always underdetermined and thus could always enable a “fitting” of experimental results.

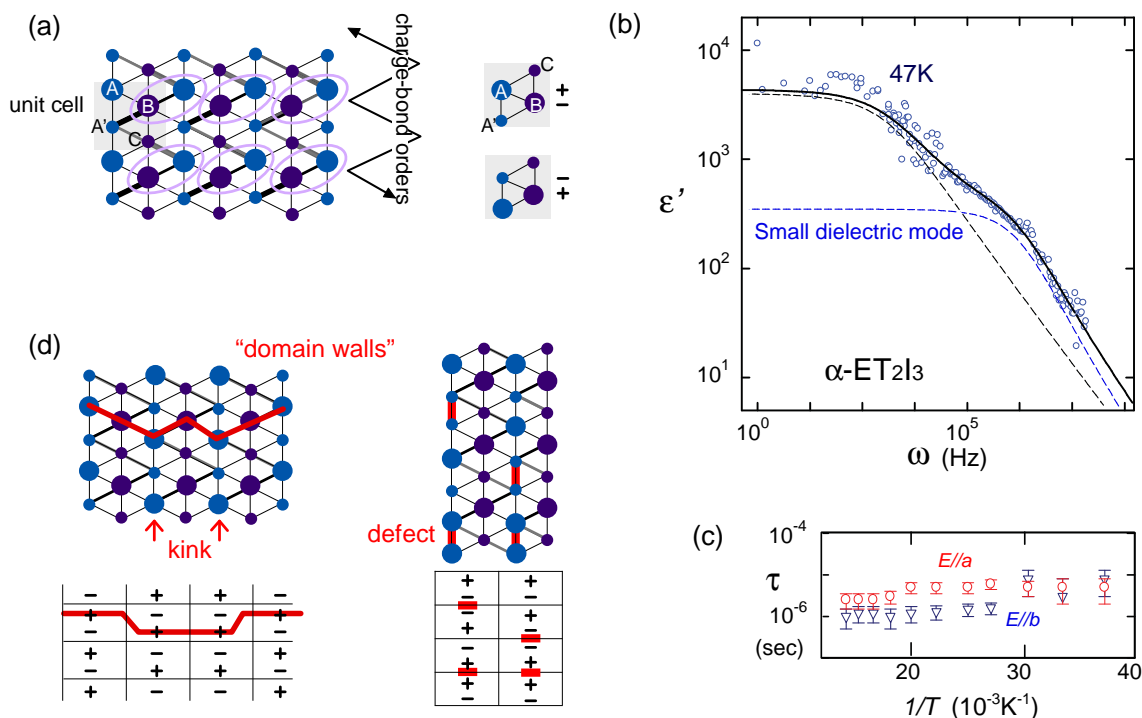
The answer to the final issue may depend on what approach one takes. The bulk coherence of the phases are lost in these materials, a situation difficult to treat in theories. We ourselves speculate from the strong coupling point of view that the disorders embedded in the frustration of V 's, which become active at finite temperature due to entropy, could be the main driving force of the intriguing events. Particularly, the “good defect state” at $V' > V$ in Figure 5(d) may overwhelm other coherent orders if coupled locally to the lattices, and bears a variation in wave vectors sensitive to the details of the materials and the environments.

5.2. Collective Charge Excitations

A distinguished example of possible collective charge excitations is proposed in α -ET₂I₃ by Ivek *et al.* [90,91]. The material has a lower crystal symmetry than the θ -type, and at the charge order transition ($T_c \sim 135$ K), the inversion is lost, which makes all the four molecules (A, A', B and C) in the unit cell inequivalent (see Figure 21(a)). The charge-bond-ordering of a $2k_F$ -period reminiscent of the charge density wave runs along the zigzag direction [92], which Hotta suggested theoretically before (Figure 20, Table.VI in [8]). The spacial structure of zigzag ordering also resembles the pair-electron crystal state reviewed in Section 4 (Figure 19(a)) $\circ=\bullet-\bullet=\circ$, while here, the bond orders are more intrinsic rather than spontaneous. Such bond order embedded in the crystal by construction allows for the finite dielectric response once the charge order sets in. Ivek *et al.* reports a rather unusual dielectric response denoted as “small dielectric mode” splitting off from other mode at $T < 75$ K, as shown in Figure 21(b). It is characterized by a short wavelength and an almost temperature independent mean relaxation time (τ in Figure 21(c)), which is in contrast to the thermally activated one-body type of behavior. Ivek *et al.* related this mode to a many body exotic charge excitation, “a domain wall” shown in Figure 21(d). Here, symbols “+” and “-” represent the polarization of charges on a pair of A and A' molecules in the unit cell, which are the two possible valence arrangements proposed by the X-ray study [92]. The domain walls are described by the phase shifts or kinks of these signs. One then finds that the two types of “domain wall” excitations along and perpendicular to the stripes are exactly the ones in the strong coupling $V' > V$ region of the anisotropic triangular lattice, which Hotta *et al.* have proposed as kinks (Figure 12(d) [25]) and defects (Figure 12(a) [42], Figures 6,7(b)), respectively. The defects in Figure 12(a) are introduced as one particle charged excitation, but it is intrinsically the same as the neutral one in Figure 7(b) and in Figure 21(d) created by moving one particle upward ($\bullet\bullet$ and $\circ\circ$), except for their excitation energy. The crystals of the α -type is more anisotropic than the lattice models we have discussed, thus the kinks of the B and C chains are not observed. The anisotropy of this crystal reflects that of t and helps to produce dielectrics, and the anisotropy of V_{ij} may remain small enough to allow for such frustration induced excitations.

While this review is focused on the organic materials, there are some relevant inorganic materials sharing common physics. Kimber *et al.* found a strong indication of the frustrated charges in Ba₃NaRu₂O₉ [93]. This metal oxides has a “quasi-molecular” crystal structure; a dimerized face-sharing octahedral Ru₂^{5.5+}O₉ forms an ideally frustrated isotropic triangular lattice. A sharp metal-insulator transition accompanied by a structural distortion at $T = 210$ K gives rise to a remarkable charge ordering; an “integer” separation of charge concentration into (Ru₂⁵⁺O₉) and (Ru₂⁶⁺O₉), which is concluded from the experimental evaluation of bond-length and by the LDA + U calculation. This is an almost classical charge ordering. They also find a melting of charge ordering by the irradiation of X-rays, which lasted for periods of several hours at low temperature. The X-rays impinging on the sample generate a low concentration of holes by the photoelectric effect, which could cause exactly the same situation found theoretically in Figure 8(a), the $1\oplus 1$ dimensional metallic state by the doping into the stripe insulator.

Figure 21. (a) Charge and bond orders of α -ET₂I₃ along the zigzag direction. The unit cell includes four independent sites, A, A', B, C, where A and A' have inversion crystallographically; (b) Dielectric constant of α -ET₂I₃ at $T = 47$ K; and (c) relaxation time of the small dielectric mode (fitted in broken lines), adapted with permission from [90], copyrighted by the American Physical Society; (d) Sketch of the configuration of charges related to the small dielectric mode. The large/small circle indicate the charge rich/poor site, and “+” and “-” are the polarization of A and A' molecules in a unit cell (see (a)).



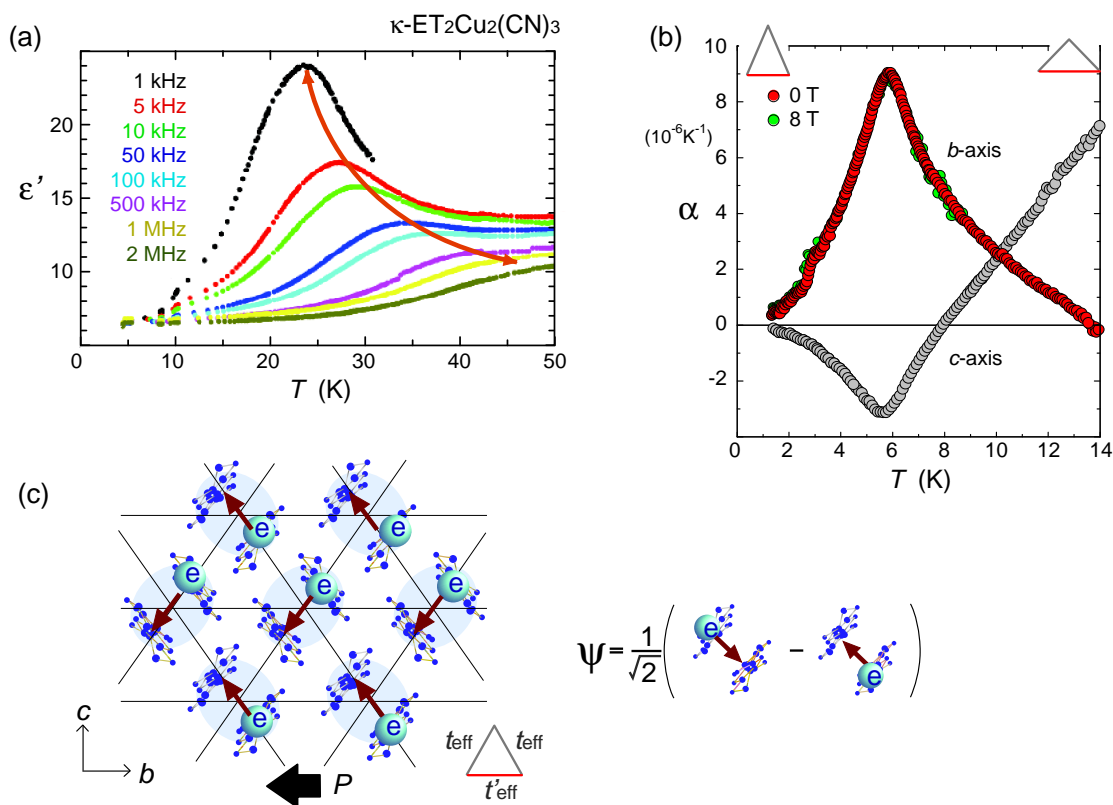
5.3. Spin Liquids, Dielectrics

Most of the strongly correlated insulators become a magnet, a spin glass, or form valence bonds (spin gapped), and at present, the only remaining possibility of realizing a triangular lattice spin liquid points toward the organic candidates, κ -(BEDT-TTF)₂Cu₂(CN)₃ [81] and EtMe₃Sb[Pd(dmit)₂]₂ [94]. Both of them are expected to have a geometry of an almost regular triangle in unit of dimer. After the ¹H-NMR study on κ -(BEDT-TTF)₂Cu₂(CN)₃ pointing out the absence of magnetic orders down to 32 mK [95], the thermodynamic measurements started to disclose the character of its low energy excitation; the specific heat shows a gapless [96] behavior, whereas the thermal transport claims that it is gapped [97], which is still controversial. The case of EtMe₃Sb[Pd(dmit)₂]₂ is also intriguing; specific heat [98] and thermal transport measurements [99] indicate a gapless excitation. On the other hand, NMR measurements indicate that there is a nodal gap [100].

Very recently, it turned out that these materials have something more than a simple quantum antiferromagnet could offer. Abdel-Jawad *et al.* [101] found a dielectric anomaly in κ -(BEDT-TTF)₂Cu₂(CN)₃ as shown in Figure 22(a); the dielectric constant ϵ' shows a broad peak structure from around 6 K to 60 K, whose peak positions depend much on the frequency, reminiscent of a relaxor ferroelectrics. The tail fitted by the Curie–Weiss law indicates a Curie temperature of $T_c = 6$ K. Such

“6K-anomaly” is already detected in the NMR susceptibility [95] and in the heat capacity [96] as humps. Manna *et al.* measured a lattice expansion coefficient [102] and showed that the uniaxial expansivities reveal a distinct upturn/downturn at 6 K (see Figure 22(b)), which could possibly be a sign of a second order phase transition. A very recent dielectric measurement by Lunkenheimer *et al.* [103] reports a more distinct transition in κ -ET₂Cu[N(CN)₂]Cl, at around 27 K from a dimer Mott insulator to charge ordering. At almost the same temperature, the long range antiferromagnetic ordering sets in, pointing toward the possibility of realizing multiferroics in the organics for the first time. Many experiments are thus ongoing, and at present, there are so many issues to be solved. (1) Is the “6 K anomaly” a phase transition or not, and is it related only to charges or also to spins?; (2) What is the ground state of the system?; (3) Do the low energy thermodynamic excitations include the charge degrees of freedom, and are they magnetic or nonmagnetic?

Figure 22. (a) Dielectric constant of a single crystal of κ -ET₂Cu₂(CN)₃ along the *a*-axis. By the courtesy of Ichiro Terasaki; (b) In-plane uniaxial expansion coefficients, $\alpha = (dl/dT)/l$ of κ -ET₂Cu₂(CN)₃ by Mana *et al.*, adapted with permission from [102], copyrighted by the American Physical Society. With decreasing temperature below 50 K, the *b*-axis contracts and the *c*-axis expands, while at 6 K the degree of expansions shows an anomaly; (c) Schematic description of the anti-binding dimer wave function ψ , which is the equal weight superposition of two configurations of the quantum electric dipoles, and the ferroelectric charge ordered state (dipolar solid) on a κ -type crystal (left panel).



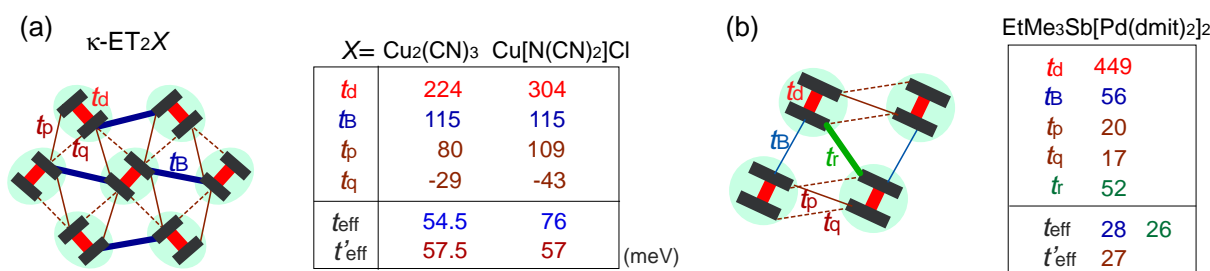
We proposed a new object, “quantum electric dipole” tightly bound to dimers, as a microscopic origin of the dielectric anomaly, which emerges in the dimer Mott insulating state [101]. The simplified description of dipoles, $\sqrt{\langle q^2 \rangle}l$, with l being the distance of dimerized molecules, gives the experimental estimate, $q = 0.1e$, from the Curie–Weiss plot of the tail of the dielectric constant. As shown in Figure 22(c), the anti-bonding wave function ψ on a dimer indicates the strong quantum fluctuation of an electric dipole. When the correlation between different dipoles develops by the Coulomb interaction V , the macroscopic ferroelectric moment P could appear. Naka and Ishihara [104] also studied the model equivalent to the dipole-spin one, by the mean field and classical Monte Carlo method, presenting a clear picture of the ferroelectric charge order (dipolar order). Gomi *et al.* showed in their calculation that these dipoles contribute to a characteristic collective mode in a terahertz frequency region [105]. Thus, the theories began to reconcile with part of the experiments. From the exact diagonalization on the dipole-spin model, Hotta even found a possible “nonmagnetic” dimer Mott phase in the vicinity of transition to a ferroelectric ordering, in which the magnetic correlation becomes structureless for all k -numbers [20]. The origin of this “spin disorder” is the direct spin-charge coupling (see also Section 3.3), different from those of Section 3.4.

The trials to reconcile the real materials with lattice models by the ab-initio downfolding calculations are performed on these material systems. Nakamura *et al.* obtained a new set of lattice parameters of the half-filled Hubbard model (in unit of dimer) for κ -ET₂Cu(NCS)₂ and κ -ET₂Cu₂(CN)₃ as $t'_{\text{eff}}/t_{\text{eff}} = 0.66$ and 0.8 , $V_{\text{eff}}/t_{\text{eff}} = 5.4$ and 6.4 , $U_{\text{eff}}/t_{\text{eff}} \sim 12$ (0.83 eV) and 15 (0.85 eV) [13]. Another ab-initio work by Kandpal *et al.* also gives the consistent estimate, $t'_{\text{eff}}/t_{\text{eff}} \sim 0.84$ [12]. These results indicate that the value of V is strong and the anisotropy is large, rather apart from the regular triangle. The thermal expansions in Figure 22(b) show that with decreasing temperature at $T < 50$ K (where the dielectric constants start to increase) [102], the b/c -axis contracts/expands, and this may roughly increase t' against t (the effect on \tilde{V} is more complicated) at lower temperature. The anomaly at 6 K may be understood in this direction, if the temperature dependence of the model parameters could be made clear. In order to perform comparative discussions, ab-initio calculations on other materials such as κ -ET₂Cu[N(CN)₂]Cl, EtMe₃Sb[Pd(dmit)₂]₂, and also the ones on the molecular-based models (not in unit of dimers) are awaited. At present, the semi-empirical evaluation of the transfer integrals at hand [14,106,107] summarized in Figure 23 provides a hint to understand the difference between materials; the degree of dimerization against other transfer integral yields $t_d/t_B \sim 2, 2.6,$ and 7 for κ -ET₂Cu₂(CN)₃, κ -ET₂Cu[N(CN)₂]Cl and EtMe₃Sb[Pd(dmit)₂]₂, respectively. For example, if one assumes $U/t_B = 10$ and $V_d/t_B = 6$, the dimer approximation in Equation (5) gives $U_{\text{eff}}/t_{\text{eff}} = 5 \sim 8$ for κ -type and 12 for the dmit salt. The charge gap should accordingly be very large in the latter. At least, we could argue that the EtMe₃Sb[Pd(dmit)₂]₂ is a “clean” Mott insulator well approximated by the single band Hubbard model, whereas κ -ET₂Cu₂(CN)₃ is a “dirty” Mott insulator since the intra-dimer degrees of freedom must be accounted for in such cases where t_d/V is relatively smaller. The origin of “the spin liquid” state may thus differ between the two.

Recently, the studies on dielectric properties of the organic materials by the optical second-harmonic generations (SHG) are developing. Yamamoto *et al.* applied this method to α -ET₂I₃ discussed in the previous subsection, and found a clear SHG signal below the charge order transition at 135 K [108,109]. They also detected a novel series of dielectric phases in α' -ET₂IBr₂ [110]; below $T \lesssim 200$ K, the

inter-layer antiferroelectric phase appears (without the SHG signal), and it turns into a ferroelectric phase at $T < 160$ K, where the SHG signal sets in. These phases, now under investigation, are possibly related to the competition of the stripe orders [110]. Such new technique have drawn attention, because of the difficulty to elucidate experimentally the proper dielectric response in a sample with relatively high conductance. Indeed, many oxides containing mixed valent cations, displaying an insulating behavior and a defect-related conductivity at the same time, could easily display high dielectric constants as an artifact of inhomogeneity induced in samples, which are not related to the bulk ferroelectric polarization—it is called the Maxwell–Wagner-type of response [111]. In frustrated systems, such inhomogeneity may easily take place, and due to the relatively small charge gap, the organic crystals could also fall into this set-up. The careful examinations in the studies of “electronic dielectrics” is now strongly demanded.

Figure 23. Transfer integrals of (a) κ -ET₂Cu₂(CN)₃ [14], κ -ET₂Cu[N(CN)₂]Cl [107] and (b) EtMe₃Sb[Pd(dmit)₂]₂ [106] by the extended Hückel method. The effective inter-dimer transfer integrals, $t_{\text{eff}} = t_B/2$ or $t_r/2$, $t'_{\text{eff}} = (t_p - t_q)/2$ or $(t_p + 2t_q)/2$ are obtained by the dimer approximation (Section 2.2).



6. Concluding Remarks

In frustrated quantum magnets, a building block of nonmagnetic states is a pair of spins forming singlets called valence bond. The spins therein are highly correlated with other spin singlets but are still strongly fluctuating, and the degree of localization of singlet pairs could be a measure of the spin gap — spanning from a gapped valence bond solid to a possibly gapless spin liquid often represented by the terminology “the resonating valence bonds”.

In the quarter-filled electronic systems, the “valence bonds” of charges on a dimer could be a key ingredient. When each charge is localized on a single “valence bond orbital” of a dimer, the charge gap opens, forming a dimer Mott insulator. If the charge gap is large enough, the electronic spins conform to a localized Heisenberg spin description. But this does not apply to the dimer Mott insulators in organic κ -ET₂X which has a much smaller Mott gap than in inorganic compounds such as High- T_c cuprates. In a “spin liquid” compound, κ -ET₂Cu₂(CN)₃, even a clear Mott gap itself is vanishing spectroscopically [112]. Such a small charge gap is a source of strong charge fluctuation; the long distance charge fluctuation allow for multiple long range spin exchange couplings, and realizes the “spin liquid Mott insulator” on an anisotropic triangular lattice as we saw in Section 3.4. Whereas a short range charge fluctuation (valence bond fluctuation) may couple the spin and charge degrees of freedom

and afford another dirty “spin liquid” in Section 3.3. We discussed κ -ET₂Cu₂(CN)₃ mainly in the latter context. These are something not attained in a laboratory study of simple frustrated magnets.

The finite structural dimerization allows for a particular classes of dielectric properties in the families of organic materials, the strongly dimerized κ -, β' -, and a weakly dimerized α -ET₂X. The dimer Mott insulator is a “strong valence bond” crystal of charges, and the charge ordered state with finite bond ordering is the one with a “weak valence bond”. The former shall yield an order-disorder type of ferroelectrics—based on the quantum electric dipoles localized on a capsule of dimers. The latter could be loosely connected with the displacement type of ferroelectrics; while driven by the Coulomb forces, the electron-lattice coupling plays important roles, and thus may yield larger dielectric moments. In both cases, the frustrations among Coulomb interactions enhance the fluctuation against the charge correlation, and melt this “ferroelectric” ordering, as we discussed in Section 3.3 and in the last part of Section 4. The field in search of such “electronic ferroelectricity”, although still suffering from many experimental difficulties, is now growing rapidly, with a hope to find something qualitatively new emerging in this regime.

Finally, the simplest form of charge frustration occurs in non-dimerized quarter-filled systems, as a competition of charge orders of numerous types of stripe textures, and as an emergence of three-fold exotic metals with coexisting solid and liquid components of charges. They are the products of frustrated Coulomb interactions, and could be a source of inhomogeneity found in the θ -ET₂X compounds. Some of their exotic many body excitations, domain-walls, nearly fractionalized particles, resonating droplets, *etc.*, could hopefully be captured in experiments (see Section 5.2) as smoking guns of charge frustration. One important issue left for future studies is the “bad metals” in the vicinity of charge ordering at finite temperature (Section 3.1). Their origin and nature are not yet understood in theories, and much less about their relation with the frustration effects. For example, their possible relevance with the transport properties needs clarification; in the metallic phase at temperatures above the charge order transition, a nearly temperature-independent conductivity is found in many organic solids.

In this way, classified by the degree of dimerization, the effects of frustrations on the quarter-filled electronic systems with strong interactions could be viewed systematically, as we proposed in the preliminaries (Figure 2(b)). Some of the readers may have already recognized that the physics from strong to weak dimerization also tunes the nature of frustration from relatively quantum to classical. This is because the dimer (valence bond of charges) is basically a pure quantum object, and charge order is a product of classical Coulomb interactions. The quantum fluctuation favors the former whereas the correlation favors the latter. Thus, the studies on the frustration effects in quarter-filled organic solids may provide some cross-sections of a fundamental problem in condensed matters. We have only touched part of the abundant phenomena expected in the physics of the frustrated electrons, but we hope that this review proves useful to researchers in the field and motivates further investigation of organic and inorganic material systems related to frustration.

Acknowledgments

I acknowledge the collaboration with Nobuo Furukawa, Satoshi Nishimoto, Frank Pollmann, Kenn Kubo, Akihiko Nakagawa, Shin Miyayara, and Mitake Miyazaki, which this review is based on. I

attained a great deal from the fruitful discussions and communications with Yoshio Nogami, Ichiro Terasaki, Takahiko Sasaki, Tetsuaki Itou, and Shinichiro Iwai. I thank Jaime Merino, Kaoru Yamamoto, Takashi Koretsune, and Martin Drressel for many helpful discussions in writing this article. During the studies related to this review, the author was supported by Grant-in-Aid for Scientific Research (No. 21110522, 19740218, 22014014) from the Ministry of Education, Science, Sports and Culture of Japan.

References

1. Wannier, G.H. Antiferromagnetism: The triangular ising net. *Phys. Rev.* **1950**, *79*, 357–364.
2. Toulouse, G. Theory of the frustration effect in spin glasses. *Commun. Phys.* **1977**, *2*, 115–120.
3. Diep, H.T. *Frustrated Spin Systems*; World Scientific: Singapore, 1994.
4. Noda, Y.; Imada, M. Quantum phase transitions to charge-ordered and wigner-crystal states under the interplay of lattice commensurability and long-range coulomb interactions. *Phys. Rev. Lett.* **2002**, *89*, doi:10.1103/PhysRevLett.89.176803.
5. Seo, H. Charge ordering in organic ET compounds. *J. Phys. Soc. Jpn.* **2000**, *69*, 805–820.
6. Kino, H.; Fukuyama, H. Electronic states of conducting organic κ -(BEDT-TTF)₂X. *J. Phys. Soc. Jpn.* **1995**, *64*, 2726–2729.
7. Seo, H.; Hotta, C.; Fukuyama, H. Toward systematic understanding of diversity of electronic properties in low dimensional molecular solid. *Chem. Rev.* **2004**, *105*, 5005–5036.
8. Hotta, C. Classification of quasi-two-dimensional organic conductors based on a new minimal model. *J. Phys. Soc. Jpn.* **2003**, *72*, 840–853.
9. Mori, T.; Kobayashi, A.; Sasaki, T.; Kobayashi, H.; Saito, G.; Inokuchi, H. The intermolecular interaction of tetrathiafulvalene and bis(ethylenedithio)tetrathiafulvalene in organic metals: Calculation of orbital overlaps and models of energy-band structures. *Bull. Chem. Soc. Jpn.* **1984**, *57*, 627–633 and references therein.
10. Miyazaki, T.; Terakura, K.; Morikawa, Y.; Yamasaki, T. First-principles theoretical study of metallic states of DCNQI-(Cu,Ag) systems: Simplicity and variety in complex systems. *Phys. Rev. Lett.* **1995**, *74*, 5104–5107.
11. Tamura, M.; Kuroda, H.; Uji, S.; Aoki, H.; Tokumoto, M.; Swanson, A.G.; Brooks, J.S.; Agosta, C.C.; Hannahs, S.T. Analysis of de Haas-van alphen oscillations and band structure of an organic superconductor, θ -(BEDT-TTF)₂I₃. *J. Phys. Soc. Jpn.* **1994**, *63*, 615–622.
12. Kandpal, H.C.; Opahle, I.; Zhang, Y.-Z.; Jeschke, H.O.; Valentí, R. Revision of model parameters for κ -type charge transfer salts: An Ab initio study. *Phys. Rev. Lett.* **2009**, *103*, doi:10.1103/PhysRevLett.103.067004.
13. Nakamura, K.; Yoshimoto, Y.; Kosugi, T.; Arita, R.; Imada, M. Ab initio derivation of low-energy model for κ -ET type organic conductors. *J. Phys. Soc. Jpn.* **2009**, *78*, doi:10.1143/JPSJ.78.083710.
14. Komatsu, T.; Masukawa, N.; Inoue, T.; Saito, G. Realization of superconductivity at ambient pressure by band-filling control in κ -(BEDT-TTF)₂Cu₂(CN)₃. *J. Phys. Soc. Jpn.* **1996**, *65*, 1340–1354.

15. Fritsch, A.; Ducasse, L. A valence-bond approach to the electronic localization in 3/4 filled systems. *J. Phys. Fr.* **1991**, *11*, 855–880.
16. Mori, T. Estimation of off-site coulomb integrals and phase diagrams of charge ordered states in the θ -phase organic conductors. *Bull. Chem. Soc. Jpn.* **2000**, *73*, 2243–2253.
17. Scriven, E.; Powell, B.J. Toward the parametrization of the Hubbard model for salts of bis(ethylenedithio)tetrathiafulvalene: A density functional study of isolated molecules. *J. Chem. Phys.* **2009**, *130*, 104508:1–104508:10.
18. Mila, F. Deducing correlation parameters from optical conductivity in the Bechgaard salts. *Phys. Rev. B* **1995**, *52*, 4788–4793.
19. In one dimension, taking $U = \infty$ in the extended Hubbard model exactly gives the t - V model as a Hamiltonian of the charge sector. In contrast, in two and three dimensions, the fermionic exchange sign requires complicated extra phases in the fermionic operator mapped from the electron operator, thus the two are only roughly, but not exactly, equivalent.
20. Hotta, C. Quantum electric dipoles in spin-liquid dimer Mott insulator, κ - $\text{ET}_2\text{Cu}_2(\text{CN})_3$. *Phys. Rev. B* **2010**, *82*, 241104:1–241104:4.
21. Feiner, L.F.; Oleś, A.M.; Zaanen, J. Quantum melting of magnetic order due to orbital Fluctuations. *Phys. Rev. Lett.* **1997**, *78*, 2799–2802.
22. Shoji, I. Statistics of kagomé lattice. *Prog. Theor. Phys.* **1951**, *6*, 306–308.
23. Corruccini, L.R.; White, S.J. Dipolar antiferromagnetism in the spin-wave approximation. *Phys. Rev. B* **1993**, *47*, 773–777.
24. Villain, J.; Bidaux, R.; Carton, J.-P.; Conte, R. Order as an effect of disorder. *J. Phys.* **1980**, *41*, 1263–1272.
25. Hotta, C.; Furukawa, N.; Nakagawa, A.; Kubo, K. Phase diagram of spinless fermions on an anisotropic triangular lattice at half-filling. *J. Phys. Soc. Jpn.* **2006**, *75*, 123704:1–123704:6.
26. Hotta, C.; Kiyota, T.; Furukawa, N. Dimensional crossover in the Ising antiferromagnet on the anisotropic triangular lattice at finite temperature. *Europhys. Lett.* **2011**, *93*, 47001:1–47001:6.
27. Nishimoto, S.; Hotta, C. Density-matrix renormalization study of frustrated fermions on a triangular lattice. *Phys. Rev. B* **2009**, *79*, 195124:1–195124:5.
28. Hotta, C.; Furukawa, N. Strong coupling theory of the spinless charges on the triangular lattices: Possible formation of a gapless charge ordered liquid. *Phys. Rev. B* **2006**, *74*, 193107:1–193107:4.
29. Miyazaki, M.; Hotta, C.; Miyahara, S.; Matsuda, K.; Furukawa, N. Variational monte carlo study of a spinless fermion t - V model on a triangular lattice: Formation of a pinball liquid. *J. Phys. Soc. Jpn.* **2009**, *78*, doi:10.1143/JPSJ.78.014707.
30. In the variational Monte Carlo study in [29], the plane wave function is used as a trial wave function, which is disadvantageous of realizing such long range order, to estimate the upper bound of the phase boundary, $V_c = V'_c \sim 12t$. The DMRG result in [27] gives the lower estimate, $V_c = V'_c \sim 6t$.
31. Cano-Cortes, L.; Ralko, A.; F'evrier, C.; Merino, J.; Fratini, S. Geometrical frustration effects on charge-driven quantum phase transitions. *Phys. Rev. B* **2011**, *80*, 155115:1–155115:13.

32. Merino, J.; Seo, H.; Ogata, M. Quantum melting of charge order due to frustration in two-dimensional quarter-filled systems. *Phys. Rev. B* **2005**, *71*, 125111:1–125111:5.
33. Watanabe, H.; Ogata, M. Mean-field study of charge order with long periodicity in θ -(BEDT-TTF)₂X. *J. Phys. Soc. Jpn.* **2006**, *75*, 063702:1–063702:4.
34. Nishimoto, S.; Shingai, M.; Ohta, Y. Coexistence of distinct charge fluctuations in θ -(BEDT-TTF)₂X. *Phys. Rev. B* **2008**, *78*, 035113:1–035113:9.
35. The VMC could afford a largest system size of $N \sim 400$ but assumes the trial wave function of a plane-wave type, and the possibility of better wave functions including more correlations always remains. At present, the DMRG result on a $N = 8 \times 6$ cluster with $m = 1400$ could determine the energy within the accuracy of $10^{-2}t$, and thus may give relatively the most reliable result, while sometimes overestimating the ordered state due to boundary effects. The later study by the exact diagonalization in [31] shows quantitatively good agreement with the DMRG results [37].
36. Kaneko, M.; Ogata, M. Mean-field study of charge order with long periodicity in θ -(BEDT-TTF)₂X. *J. Phys. Soc. Jpn.* **2006**, *75*, 014710:1–014710:6.
37. Nishimoto, S. Leibniz Institute for Solid State and Materials Research, Dresden, Germany. Private communication, 2012.
38. Cano-Cortes, L.; Merino, J.; Fratini, S. Quantum critical behavior of electrons at the edge of charge order. *Phys. Rev. Lett.* **2010**, *105*, 036405:1–036405:4.
39. Merino, J. Universidad Autonoma de Madrid, Spain. Private communication, 2012.
40. Dressel, M. Quantum criticality in organic conductors? Fermi liquid versus non-Fermi-liquid behaviour. *J. Phys.* **2011**, *23*, doi:10.1088/0953-8984/23/29/293201.
41. Amaricci, A.; Camjayi, A.; Haule, K.; Kotliar, G.; Tanasković, D.; Dobrosavljević, V. Extended hubbard model: Charge ordering and wigner-mott transition. *Phys. Rev. B* **2010**, *82*, 155102:1–155102:10.
42. Hotta, C.; Pollmann, F. Dimensional tuning of electronic states under strong and frustrated interactions. *Phys. Rev. Lett.* **2008**, *100*, 186404:1–186404:4.
43. Hubbard, J. Generalized Wigner lattices in one dimension and some applications to tetracyanoquinodimethane (TCNQ) salts. *Phys. Rev. B* **1978**, *17*, 494–505.
44. Mayr, M.; Horsch, P. Domain-wall excitations and optical conductivity in one-dimensional Wigner lattices. *Phys. Rev. B* **2006**, *73*, 195103:1–195103:15.
45. Tanaka, Y.; Yonemitsu, K. Effects of electron-lattice coupling on charge order in θ -BEDT-TTF₂X. *J. Phys. Soc. Jpn.* **2007**, *76*, 053708:1–053708:5.
46. Fratini, S.; Merino, J. Unconventional metallic conduction in two-dimensional Hubbard-Wigner lattices. *Phys. Rev. B* **2009**, *80*, 165110:1–165110:9.
47. Pietig, R.; Bulla, R.; Blawid, B. Reentrant charge order transition in the extended hubbard model. *Phys. Rev. Lett.* **1999**, *82*, 4046–4049.
48. Merino, J. Nonlocal coulomb correlations in metals close to charge order insulator transition. *Phys. Rev. Lett.* **2007**, *99*, 036404:1–036404:4.
49. Nad, F.; Monceau, P. Dielectric response of the charge ordered state in quasi-one-dimensional organic conductors. *J. Phys. Soc. Jpn.* **2006**, *75*, 051005:1–051005:12.

50. Van den Brink, J.; Khomskii, D.I. Multiferroicity due to charge ordering. *J. Phys.* **2008**, *20*, doi:10.1088/0953-8984/20/43/434217.
51. Yoshioka, H.; Tsuchiizu, M.; Seo, H. Charge-ordered state versus dimer-mott insulator at finite temperatures. *J. Phys. Soc. Jpn.* **2007**, *76*, 103701:1–103701:4.
52. Tsuchiizu, M.; Yoshioka, H.; Suzumura, Y. Crossover from quarter-filling to half-filling in a one-dimensional electron system with a dimerized and quarter-filled band. *J. Phys. Soc. Jpn.* **2001**, *70*, 1460–1463.
53. Anderson, P.W. Resonating valence bonds: A new kind of insulator ? *Mat. Res. Bull.* **1973**, *8*, 153–160.
54. Bernu, B.; Lhuillier, C.; Pierre, L. Signature of neel order in exact spectra of quantum antiferromagnets on finite lattices. *Phys. Rev. Lett.* **1992**, *69*, 2590–2593.
55. Capriotti, L.; Trumper, A.E.; Sorella, S. Long-range neel order in the triangular heisenberg model. *Phys. Rev. Lett.* **1999**, *82*, 3899–3902.
56. Trumper, A.E. Spin-wave analysis to the spatially anisotropic Heisenberg antiferromagnet on a triangular lattice. *Phys. Rev. B.* **1999**, *60*, 2987–2989.
57. Weihong, Z.; McKenzie, R.H. Phase diagram for a class of spin-1/2 Heisenberg models interpolating between the square-lattice, the triangular-lattice, and the linear-chain limits. *Phys. Rev. B* **1999**, *59*, 14367–14375.
58. Misguich, G.; Lhuillier, C.; Bernu, B.; Waldtmann, C. Spin-liquid phase of the multiple-spin exchange Hamiltonian on the triangular lattice. *Phys. Rev. B* **1999**, *60*, 1064–1074.
59. Morita, H.; Watanabe, S.; Imada, M. Nonmagnetic insulating states near the mott transitions on lattices with geometrical frustration and implications for κ -(ET)₂Cu₂(CN)₃. *J. Phys. Soc. Jpn.* **2002**, *71*, doi:10.1143/JPSJ.71.2109.
60. Koretsune, T.; Motome, Y.; Furusaki, A. Exact diagonalization study of mott transition in the hubbard model on an anisotropic triangular lattice. *J. Phys. Soc. Jpn.* **2007**, *76*, doi:10.1143/JPSJ.76.074719.
61. Kyung, B.; Tremblay, A.-M.S. Mott transition, antiferromagnetism, and d-wave superconductivity in two-dimensional organic conductors. *Phys. Rev. Lett.* **2006**, *97*, 046402:1–046402:4.
62. Clay, R.T.; Li, H.; Mazumdar, S. Absence of superconductivity in the half-filled band hubbard model on the anisotropic triangular lattice. *Phys. Rev. Lett.* **2008**, *101*, 166403:1–166403:4.
63. Yoshioka, T.; Koga, A.; Kawakami, N. Quantum phase transitions in the hubbard model on a triangular lattice. *Phys. Rev. Lett.* **2009**, *103*, 036401:1–036401:4.
64. Kino, H.; Kontani, H. Phase Diagram of Superconductivity on the Anisotropic Triangular Lattice Hubbard Model: An Effective Model of κ -(BEDT-TTF) Salts. *J. Phys. Soc. Jpn.* **1998**, *67*, 3691–3694.
65. Liu, J.; Schmalian, J.; Trivedi, N. Pairing and superconductivity driven by strong quasiparticle renormalization in two-dimensional organic charge transfer salts. *Phys. Rev. Lett.* **2005**, *94*, 127003:1–127003:4.
66. Watanabe, T.; Yokoyama, H.; Tanaka, Y.; Inoue, J. Superconductivity and a mott transition in a hubbard model on an anisotropic triangular lattice. *J. Phys. Soc. Jpn.* **2006**, *75*, 074707:1–074707:15.

67. Dayal, S.; Clay, R.T.; Mazumdar, S. Absence of long-range superconducting correlations in the frustrated half-filled-band Hubbard model. *Phys. Rev. B* **2012**, *85*, 165141:1–165141:8.
68. The VMC calculation by Watanabe *et al.* [66] shows that the quasiparticle renormalization factor shows a jump at the transition from a *d*-SC to the Mott insulator, and its magnitude is enhanced with increasing t'/t . This fact is in agreement with the *d*-SC to NMI transition detected as a jump in the double occupancy by Kyung and Tremblay (CDMFT) [61].
69. Mizusaki, T.; Imada, M. Gapless quantum spin liquid, stripe, and antiferromagnetic phases in frustrated Hubbard models in two dimensions. *Phys. Rev. B* **2006**, *74*, 014421:1–014421:10.
70. Yang, H.-Y.; Läuchli, A.M.; Mila, F.; Schmidt, K.P. Effective spin model for the spin-liquid phase of the hubbard model on the triangular lattice. *Phys. Rev. Lett.* **2010**, *105*, 267204:1–267204:4.
71. Lee, S.-S.; Lee, P.A. U(1) gauge theory of the Hubbard model: Spin liquid states and possible application to κ -(BEDT-TTF)₂Cu₂(CN)₃. *Phys. Rev. Lett.* **2005**, *95*, 036403:1–036403:4.
72. Ramirez, A.P. A flood or a trickle? *Nat. Phys.* **2008**, *4*, 442–443.
73. Motrunich, O.I. Variational study of triangular lattice spin-1/2 model with ring exchanges and spin liquid state in κ -ET₂Cu₂(CN)₃. *Phys. Rev. B* **2005**, *72*, 045105:1–045105:7.
74. Zlatić, V.; Entel, P.; Grabowski, S. Spectral properties of two-dimensional Hubbard model with anisotropic hopping. *Europhys. Lett.* **1996**, *34*, 693–698.
75. Yoshimi, K.; Kato, T.; Maebashi, H. Fermi surface deformation near charge-ordering transition. *J. Phys. Soc. Jpn.* **2011**, *80*, 123707:1–123707:4.
76. Udagawa, M.; Motome, Y. Charge ordering and coexistence of charge fluctuations in quasi-two-dimensional organic conductors θ -BEDT-TTF₂X. *Phys. Rev. Lett.* **2007**, *98*, 206405:1–206405:4.
77. Watanabe, M.; Noda, Y.; Nogami, Y.; Mori, H. Transfer Integrals and the Spatial Pattern of Charge Ordering in θ -(BEDT-TTF)₂RbZn(SCN)₄ at 90K. *J. Phys. Soc. Jpn.* **2004**, *73*, 116–122.
78. Tanaka, Y.; Yonemitsu, K. Nonlinear conduction by melting of stripe-type charge order in organic conductors with triangular lattices. *J. Phys. Soc. Jpn.* **2011**, *80*, 103702:1–103702:4.
79. Dayal, S.; Clay, T.; Li, H.; Mazumdar, S. Paired electron crystal: Order from frustration in the quarter-filled band. *Phys. Rev. B* **2011**, *83*, 245106:1–245106:12.
80. Otsuka, Y.; Seo, H.; Motome, Y.; Kato, T. Finite-temperature phase diagram of quasi-one-dimensional molecular conductors: Quantum monte carlo study. *J. Phys. Soc. Jpn.* **2008**, *77*, 113705:1–113705:4.
81. Kanoda, K. Metal-insulator transition in κ -(ET)₂X and (DCNQI)₂M: Two contrasting manifestation of electron correlation. *J. Phys. Soc. Jpn.* **2006**, *75*, 051007:1–051007:16.
82. Kuroki, K. Theoretical aspects of charge correlations in θ -(BEDT-TTF)₂X. *Sci. Technol. Adv. Mater.* **2009**, *10*, 024312:1–024312:11 and the references therein.
83. Sawano, F.; Terasaki, I.; Mori, H.; Mori, H.; Watanabe, M.; Ikeda, N.; Nogami, Y.; Noda, Y.F.; Sawano, I.; Terasaki, H.; *et al.* An organic thyristor. *Nature* **2005**, *437*, 522–524.
84. Miyagawa, K.; Kawamoto, A.; Kanoda, K. Charge ordering in a quasi-two-dimensional organic conductor. *Phys. Rev. B* **2000**, *62*, R7679–R7682.
85. Sawano, F.; Suko, T.; Inada, T.S.; Tasaki, S.; Terasaki, I.; Mori, H.; Nogami, Y.; Ikeda, N.; Watanabe, M.; *et al.* Current-density dependence of the charge-ordering gap in the organic

- salt θ -(BEDT-TTF)₂CsZn(SCN)₄ ($M = \text{Zn, Co, Co}_{0.7}\text{Zn}_{0.3}$). *J. Phys. Soc. Jpn.* **2009**, *78*, 024714:1–024714:5.
86. Nogami, Y.; Hanasaki, N.; Watanabe, M.; Yamamoto, K.; Ito, T.; Ikeda, N.; Ohsumi, H.; Toyokawa, H.; Noda, Y.; Terasaki, I.; *et al.* Charge order competition leading to nonlinearity in organic thyristor family. *J. Phys. Soc. Jpn.* **2010**, *79*, 044606:1–044606:5.
87. Yukawa, E.; Ogata, M. Mean-field analysis of electric field effect on charge orders in organic conductors. *J. Phys. Soc. Jpn.* **2010**, *79*, 023705:1–023705:4.
88. Inagaki, K.; Terasaki, I.; Mori, H.; Mori, T. Large dielectric constant and giant nonlinear conduction in the organic conductor θ -(BEDT-TTF)₂CsZn(SCN)₄. *J. Phys. Soc. Jpn.* **2004**, *73*, 3364–3369.
89. Kuroki, K. The origin of the charge ordering and its relevance to superconductivity in θ -(BEDT-TTF)₂X: The effect of the fermi surface nesting and the distant electron-electron interactions. *J. Phys. Soc. Jpn.* **2006**, *75*, 114716:1–114716:14.
90. Ivek, T.; Korin-Hamzic, B.; Milat, O.; Tomic, S.; Clauss, C.; Drichko, N.; Schweitzer, D.; Dressel, M. Collective excitations in the charge-ordered phase of α -(BEDT-TTF)₂I₃. *Phys. Rev. Lett.* **2010**, *104*, 206406:1–206406:4.
91. Ivek, T.; Korin-Hamzic, B.; Milat, O.; Tomic, S.; Clauss, C.; Drichko, N.; Schweitzer, D.; Dressel, M. Electrodynamic response of the charge ordering phase: Dielectric and optical studies of α -(BEDT-TTF)₂I₃. *Phys. Rev. B* **2011**, *83*, 165128:1–165128:13.
92. Kakiuchi, T.; Wakabayashi, Y.; Sawa, H.; Takahashi, T.; Nakamura, Y. Charge ordering in α -(BEDT-TTF)₂I₃ by synchrotron X-ray diffraction. *J. Phys. Soc. Jpn.* **2007**, *76*, 113702:1–113702:4.
93. Kimber, S.A.J.; Senn, M.S.; Fratini, S.; Wu, H.; Hill, A.H.; Manuel, P.; Attfield, J.P.; Argyriou, D.N.; Henry, P.F. Charge order at the frontier between the molecular and solid states in Ba₃NaRu₂O₉. *Phys. Rev. Lett.* **2012**, *108*, 217205:1–217205:4.
94. Kato, R. Conducting metal dithiolene complexes: Structural and electronic properties. *Chem. Rev.* **2004** *104*, 5319–5346.
95. Shimizu, Y.; Miyagawa, K.; Kanoda, K.; Maesato, M.; Saito, G. Spin liquid state in an organic mott insulator with a triangular lattice. *Phys. Rev. Lett.* **2003**, *91*, 107001:1–107001:4.
96. Yamashita, S.; Nakazawa, Y.; Oguni, M.; Oshima, Y.; Nojiri, H.; Shimizu, Y.; Miyagawa, K.; Kanoda, K. Thermodynamic properties of a spin-1/2 spin-liquid state in a κ -type organic salt. *Nat. Phys.* **2008**, *4*, 459–462.
97. Yamashita, M.; Nakata, N.; Kasahara, Y.; Sasaki, T.; Yoneyama, N.; Kobayashi, N.; Fujimoto, S.; Shibauchi, T.; Matsuda, Y. Thermal-transport measurements in a quantum spin-liquid state of the frustrated triangular magnet κ -(BEDT-TTF)₂Cu₂(CN)₃. *Nat. Phys.* **2008**, *5*, 44–47.
98. Yamashita, S.; Yamamoto, T.; Nakazawa, Y.; Tamura, M.; Kato, R. Gapless spin liquid of an organic triangular compound evidenced by thermodynamic measurements. *Nat. Commun.* **2011**, *2*, doi:10.1038/ncomms1274.
99. Yamashita, M.; Nakata, N.; Senshu, Y.; Nagata, M.; Yamamoto, H.M.; Kato, R.; Shibauchi, T.; Matsuda, Y. Highly mobile gapless excitations in a two-dimensional candidate quantum spin liquid. *Science* **2010**, *328*, 1246–1248.

100. Itou, T.; Oyamada, A.; Maegawa, S.; Kato, R. Instability of a quantum spin liquid in an organic triangular-lattice antiferromagnet. *Nat. Phys.* **2010**, *6*, 673–676.
101. Abdel-Jawad, M.; Terasaki, I.; Sasaki, T.; Yoneyama, N.; Kobayashi, N.; Uesu, Y.; Hotta, C. Anomalous dielectric response in the dimer Mott insulator κ -(BEDT-TTF)₂Cu₂(CN)₃. *Phys. Rev. B* **2010**, *82*, 125119:1–125119:5.
102. Manna, R.S.; de Souza, M.; Brühl, A.; Schlueter, J.A.; Lang, M. Lattice effects and entropy release at the low-temperature phase transition in the spin-liquid candidate κ -(BEDT-TTF)₂Cu₂(CN)₃. *Phys. Rev. Lett.* **2010**, *104*, 016403:1–016403:4.
103. Lunkenheimer, P.; Müller, J.; Krohns, S.; Schrettle, F.; Loidl, A.; Hartmann, B.; Rommel, R.; de Souza, M.; Hotta, C.; Schlueter, J.A.; Lang, M. Multiferroicity in an organic charge-transfer salt: Electric-dipole-driven magnetism. *Nat. Mater.* **2012**, doi:10.1038/NMAT3400
104. Naka, M.; Ishihara, S. Electronic ferroelectricity in a dimer mott insulator. *J. Phys. Soc. Jpn.* **2010**, *79*, 063707:1–063707:4.
105. Gomi, H.; Imai, T.; Takahashi, A.; Aihara, M. Purely electronic terahertz polarization in dimer Mott insulators. *Phys. Rev. B* **2010**, *82*, 035101:1–035101:7.
106. Kato, R.; Hengbo, C. Cation dependence of crystal structure and band parameters in a series of molecular conductors, β' -(Cation)[Pd(dmit)₂]₂ (dmit = 1,3-dithiole-2-thione-4,5-dithiolate). *Crystals* **2012**, *2*, 861–874.
107. Watanabe, M.; Nogami, Y.; Oshima, K.; Ito, H.; Ishiguro, T.; Saito, G. Low temperature superstructure and transfer integrals in κ -(BEDT-TTF)₂Cu[N(CN)₂]X: X = Cl, Br. *Synth. Metals* **1999**, *103*, 1909–1910.
108. Yamamoto, K.; Iwai, S.; Boyko, S.; Kashiwazaki, A.; Hiramatsu, F.; Okabe, C.; Nishi, N.; Yakushi, K. Strong optical nonlinearity and its ultrafast response associated with electron ferroelectricity in an organic conductor. *J. Phys. Soc. Jpn.* **2008**, *77*, 074709:1–074709:6.
109. Yamamoto, K.; Kowalska, A.A.; Yakushi, K. Direct observation of ferroelectric domains created by Wigner crystallization of electrons in α -[bis(ethylenedithio)tetrathiafulvalene]₂I₃. *Appl. Phys. Lett.* **2010**, *96*, 122901:1–122901:3.
110. Yamamoto, K. Institute for Molecular Science, Okazaki, Japan. Private Communication, 2012.
111. Catalan, G.; Scott, J.F. Is CdCr₂S₄ a multiferroic relaxor? *Nature* **2007**, *448*, E4–E5,
112. Kezsmarki, I.; Shimizu, Y.; Mihály, G.; Tokura, Y.; Kanoda, K.; Saito, G. Depressed charge gap in the triangular-lattice Mott insulator, κ -(ET)₂Cu₂(CN)₃. *Phys. Rev. B* **2006**, *74*, R201101:1–R201101:14.